The Cryosphere Discuss., 8, 5375–5432, 2014
www.the-cryosphere-discuss.net/8/5375/2014/
doi:10.5194/tcd-8-5375-2014

The Cryosphere Discussions
Open Access

Modelling glacier change in the Everest region, Nepal Himalaya

J. M. Shea[1], W. W. Immerzeel[1,2], P. Wagnon[1,3], C. Vincent[4], and S. Bajracharya[1]

[1]International Centre for Integrated Mountain Development, Kathmandu, Nepal
[2]Department of Physical Geography, Utrecht University, Utrecht, the Netherlands
[3]IRD/UJF – Grenoble 1/CNRS/G-INP, LTHE – UMR5564, LGGE – UMR5183, 38402 Grenoble, France
[4]UJF – Grenoble 1/CNRS, Laboratoire de Glaciologie et Géophysique de l'Environnement, LGGE – UMR5183, 38041 Grenoble, France

Received: 1 September 2014 – Accepted: 1 October 2014 – Published: 17 October 2014

Correspondence to: J. M. Shea (joseph.shea@icimod.org)

Published by Copernicus Publications on behalf of the European Geosciences Union.

Abstract

In this study, we apply a glacier mass balance and ice redistribution model to simulate historical and future glacier change in the Everest region of Nepal. High-resolution temperature and precipitation fields derived from gridded APHRODITE data, and validated against independent station observations from the EVK2CNR network, are used to drive the historical model from 1961 to 2007. The model is calibrated against geodetically derived estimates of net glacier mass change from 1992 to 2008, termini position of four large glaciers at the end of the calibration period, average velocities observed on selected debris-covered glaciers, and total glacierized area. We integrate field-based observations of glacier mass balance and ice thickness with remotely-sensed observations of decadal glacier change to validate the model. Between 1961 and 2007, the mean modelled volume change over the Dudh Kosi basin is $-6.4 \pm 1.5\,\mathrm{km}^3$, a decrease of 15.6 % from the original estimated ice volume in 1961. Modelled glacier area change between 1961 and 2007 is $-101.0 \pm 11.4\,\mathrm{km}^2$, a decrease of approximately 20 % from the initial extent. Scenarios of future climate change, based on CMIP5 RCP4.5 and RCP8.5 end members, suggest that glaciers in the Everest region will continue to lose mass through the 21st century. Glaciers in the basin are concentrated between 5000 and 6000 m of elevation, and are thus expected to be sensitive to changes in temperature and equilibrium line altitude (ELA). Glacier volume reductions between −35 to −62 % are possible by 2050, and sustained temperature increases to 2100 may result in total glacier volume losses of between −73 and −96 %.

1 Introduction

High-elevation snow and ice cover play pivotal roles in Himalayan hydrologic systems (e.g. Viviroli et al., 2007; Immerzeel et al., 2010; Racoviteanu et al., 2013). In the monsoon-affected portions of the Himalayas, meltwater from seasonal snowpacks and glaciers provides an important source of streamflow during pre- and post-monsoon

TCD
8, 5375–5432, 2014

seasons, while rainfall induced runoff during the monsoon dominates the overall hydrologic cycle (Immerzeel et al., 2013). Against this backdrop, changes in glacier area and volume are expected to have large impacts on the availability of water during the dry seasons (Immerzeel et al., 2010), which will impact agriculture, hydropower generation, and local water resources availability. In the current study, our main objectives are to calibrate and test a model of glacier mass balance and redistribution, and to present scenarios of catchment-scale future glacier evolution in the Everest region.

1.1 Study area and climate

The (ICIMOD, 2011) inventory indicates that the Dudh Kosi (or Koshi) basin in central Nepal contains a total glacierised area of approximately 410 km^2. The region contains some of the world's highest mountain peaks, including Sagarmatha (Mt. Everest), Cho Oyu, Makalu, Lhotse, and Nuptse. The Dudh Kosi River is a major contributor to the Kosi River, which contains nearly one quarter of Nepal's exploitable hydroelectric potential. Approximately 110 km^2, or 25 % of the total glacierized area, is classified as debris-covered (Fig. 2), with surface melt rates that are typically lower than those observed on clean glaciers due to the insulating effect of the debris (Reid and Brock, 2010; Lejeune et al., 2013).

The climate of the region is characterized by pronounced seasonality of both temperature and precipitation. At 5000 m (see analysis below), mean daily temperatures range between −7 and +10 °C, with minimum and maximum daily temperatures ranging between −25 and +10 °C. During the monsoon period (June–September), temperatures at 5000 m are greater than 0 °C and variability is low. The majority of annual precipitation (approximately 77 %, derived from gridded climate fields, see below) falls between June and October during the summer monsoon (Wagnon et al., 2013). An additional 14 % of precipitation occurs during the pre-monsoon period (March–May), with little or no precipitation during the post-monsoon and winter seasons. The interaction between moisture advected from the Indian Ocean during the monsoon and the two-step topography of the Dudh Kosi region (foothills, main ranges) results in two spatial maxima

TCD
8, 5375–5432, 2014

of precipitation (Bookhagen and Burbank, 2006). The first maximum occurs along the southern margin of the Himalayan foothills at approximately 900 m, while a secondary peak occurs at approximately 2100 m (Bookhagen and Burbank, 2010).

1.2 Himalayan glaciology

The current status of glaciers varies across the Hindu Kush-Himalayan (HKH) region. Most areas have seen pronounced glacier retreat and downwasting in recent years (Bolch et al., 2012; Kääb et al., 2012; Yao et al., 2012), though some areas, such as the Karakoram and Pamir ranges, have experienced equilibrium or even slight mass gain (Gardelle et al., 2012, 2013; Jacob et al., 2012). In the Everest region (Fig. 1), Gardelle et al. (2013) find an average annual rate of mass loss of -0.26 ± 0.13 m w.e. yr^{-1} between 2000 and 2011, while Nuimura et al. (2012) estimate mass loss rates of -0.40 ± 25 m w.e. yr^{-1} between 1992 and 2008. Between 2003 and 2009, thinning rates of -0.40 m yr^{-1} were estimated from ICEsat data (Gardner et al., 2013), which is consistent with an average thinning rate of -0.33 m yr^{-1} calculated over the period 1962 to 2002 for glaciers in the Khumbu region (Bolch et al., 2008a, b). Areal extents of glaciers in Sagarmatha National Park decreased 5 % during the second half of the 20th century (Bolch et al., 2008b; Salerno et al., 2008).

One consequence of glacier retreat in the Himalayas is the formation of proglacial lakes, which may pose a risk to downstream communities. Terminus retreat at Lumding and Imja glaciers, measured at -42 and -34 m yr^{-1}, respectively, between 1976 and 2000 increased to -74 m yr^{-1} at both glaciers between 2000 and 2007 (Bajracharya and Mool, 2010). Rapid terminus retreat results in the growth of proglacial lakes which are dammed by lateral and terminal moraines (Bolch et al., 2008b; Benn et al., 2012; Thompson et al., 2012). The failure of moraine dams in the Kosi River basin has led to 15 recorded glacier lake outburst flood (GLOF) events since 1965, with flows up to 100 times greater than average annual flow (Chen et al., 2013), and the frequency of GLOFs in the Himalayas is believed to have increased since the 1940s (Richardson and Reynolds, 2000). Changes in glacier extents and volumes in response to climate

TCD
8, 5375–5432, 2014

change thus have important impacts not only on water resources availability but also on geophysical hazards.

The climate sensitivity of a glacier depends primarily on its mass balance amplitude. Glaciers in wetter climates typically extend to lower elevations, and are thus more sensitive to temperature changes than those in dry climates (Oerlemans and Fortuin, 1992). Himalayan glaciers, and glaciers of the Dudh Kosi in particular, present a unique challenge as observations of temperature and precipitation at high elevations are scarce. Regionally, the climate varies from monsoon-dominated southern slopes to relatively dry leeward high-elevation regions. Accordingly, equilibrium line altitudes (ELAs) in the region vary both spatially and temporally, but generally range from 5200 m in the south to 5800 m in northern portions of the basin (Williams, 1983; Asahi, 2010; Wagnon et al., 2013). Nearly 80 % of the glacierized area in the Dudh Kosi basin lies between 5000 and 6000 m (Fig. 2), and the region is expected to be sensitive to climatic changes.

1.3 Historical and projected climate trends

Analyses of climate records in the region are limited, primarily due to the lack of long-term records (Shrestha and Aryal, 2011). Available studies indicate that the mean annual temperatures have increased in the region, and particularly at high elevations (Shrestha et al., 1999; Rangwala et al., 2009; Ohmura, 2012; Rangwala and Miller, 2012). Reported mean annual temperature trends range between 0.025 and 0.06 $^{\circ}$C yr^{-1} for the periods 1971 to 2009 and 1977 to 1994, respectively (Shrestha and Aryal, 2011; Qi et al., 2013). Changes in temperature are particularly important for monsoon-type glaciers, which are sensitive to the elevation of the rain/snow threshold during the monsoon season (Bolch et al., 2012). Results from CMIP5 ensembles suggest that temperatures in the region will increase between 1.3 and 2.4 $^{\circ}$C over the period 1961–1990 to 2021–2050 (Lutz et al., 2012), which correspond to rates of 0.021 to 0.040 $^{\circ}$C yr^{-1}.

TCD
8, 5375–5432, 2014

Precipitation amounts, timing, and phase will affect glacier responses on both annual and decadal timescales. In the greater Himalayas, trends in precipitation totals appear to be mixed and relatively weak (Mirza et al., 1998; Gautam et al., 2010; Dimri and Dash, 2012; Qi et al., 2013), though the observational network is composed mostly of low-elevation valley stations that may not reflect changes in snowfall amounts at higher elevations. General circulation model projections suggest both increased monsoon precipitation (Kripalani et al., 2007) and delayed monsoon onset (Ashfaq et al., 2009; Mölg et al., 2012) in the 21st century, while the change in total annual precipitation is mixed. In the Himalayas, CMIP5 ensembles show projected changes in precipitation between −8 to +15 % (Lutz et al., 2012; Palazzi et al., 2013).

1.4 Models of glacier change

In spite of the recent observed changes in glaciers in the Everest region, the reported climatic trends, the expected glacier sensitivity to climatic change, and the importance of glacier water resources in the region, few studies have attempted to model the historical or future response of these glaciers to climate change (Immerzeel et al., 2012, 2013). Empirical mass balance and snow and ice melt models have been developed from field observations (Ageta and Higuchi, 1984; Ageta and Kadota, 1992; Nakawo et al., 1999) and reanalysis products (Fujita and Nuimura, 2011; Rasmussen, 2013), and such approaches have been used to quantify glacier contributions to streamflow (Racoviteanu et al., 2013; Nepal et al., 2014). Projections of higher ELAs in the region (Fujita and Nuimura, 2011) and volume area-scaling approaches (Shi and Liu, 2000; Cogley, 2011) indicate continued mass wastage in the future, yet impact studies on the response of glaciers to climate change require models that link mass balance processes with representations of glacier dynamics.

One and two-dimensional models of glacier dynamics have been applied previously to the Khumbu Glacier (Naito et al., 2000) and the East Rongbuk Glacier (Zhang et al., 2013), respectively. However, these and higher-order models of glacier dynamics are severely limited by input data availability (e.g. bed topography, ice temperatures, basal

TCD
8, 5375–5432, 2014

water pressure) and uncertainties in key model parameters, and have not been applied at catchment scales in the region. Relatively coarse methods of simulating future glacier change (e.g. Stahl and Moore, 2006) can be improved by applying models that can reasonably simulate key glaciological parameters (thickness, velocity, and mass redistribution). The glacier mass balance and redistribution model described in this study is calibrated using available field and remotely-sensed observations, and tested against observed glacier changes, glacier mass balance, and ice thicknesses observations. We then develop first-order scenarios of future glacier change in the Everest region with calibrated model parameters and a suite of prescribed temperature and precipitation changes from CMIP5 downscaling ensembles.

2 Data and methods

2.1 Daily climate fields

There are few observations of temperature and precipitation in the basin, and no temperature records longer than 15 year are available. To generate high-resolution fields of temperature (T) and precipitation (P) as inputs to the model, we use data from the APHRODITE (Asian Precipitation – Highly-Resolved Observational Data Integration Towards Evaluation of Water Resources) project (Yatagai et al., 2009, 2012). APHRODITE products have been previously used to test regional climate model simulations in northern India (Mathison et al., 2013) and the western Himalaya (Dimri et al., 2013), and to compare precipitation datasets in the Himalayan region (Palazzi et al., 2013). For this study, we use APHRODITE T fields (V1204R1) that are based on daily station anomalies from climatological means, interpolated on 0.05° grids and then resampled to 0.25° fields and we refer to Yatagai et al. (2012) for more details. The APHRODITE P fields (V1101) are based on a similar technique using precipitation ratios, but incorporate a weighted interpolation scheme based on topographical considerations (Yatagai et al., 2012).

TCD
8, 5375–5432, 2014

To generate high-resolution fields of T and P for the glacier mass balance model, we extract a 14 × 14 subset of the daily APHRODITE T and P fields that covers the Kosi basin (Fig. 1). Approximate elevations for each 0.25° grid cell are extracted from a re-sampled Shuttle Radar Topography Mission (SRTM; Farr et al., 2007) digital elevation model (DEM). Based on this subset we derive relations between elevation and temperature and precipitation respectively at coarse resolution. We then use these relations in combination with 90 m SRTM DEM to produce high resolution daily climate fields.

2.1.1 Temperature

Downscaled temperature fields at daily 90 m resolution are computed as:

$$T_Z = \gamma_T Z + T_0 - C_{\mathrm{DOY}} \quad (1)$$

where γ_T is the daily vertical temperature gradient (Fig. 3) derived from the 0.25° APRHODITE temperatures and SRTM elevations, T_0 is the daily temperature intercept, and C_{DOY} is a bias correction based on the day of year (Fig. 4). The bias-correction factor is computed from the mean daily temperature difference between observed and estimated mean daily temperatures at all four EVK2CNR stations, which are independent of the APHRODITE product.

2.1.2 Precipitation

To calculate high-resolution daily precipitation fields from the APHRODITE subset, we prescribe daily precipitation-elevation functions from the 0.25° APHRODITE precipitation fields and resampled SRTM data. For each day, we calculate the mean precipitation in 500 m elevation bins ($\overline{P}_{500}$), and prescribe a fitted linear interpolation function to estimate precipitation on the 90 m SRTM DEM (Fig. 5).

As APHRODITE fields are based on interpolated station data (Yatagai et al., 2012), there is a large uncertainty in the precipitation at high elevations. Independent tests of the precipitation downscaling approach were conducted by comparing precipitation

TCD
8, 5375–5432, 2014

observations from the EVK2CNR stations with precipitation estimated using the station elevation and the daily precipitation-elevation functions (Fig. 6). As the EVK2CNR stations are not capable of measuring solid precipitation (Wagnon et al., 2013), we only examine days where only liquid precipitation ($T > 0$) is expected.

While orographic forcing of moist air masses typically produces increased precipitation with elevation, in very high elevation regions (i.e. those greater than 4000 m) both observations and models indicate that precipitation totals will decrease above a certain elevation (Harper and Humphrey, 2003; Mölg et al., 2009). This is due in part to the drying effect from upwind orographic forcing, but is also related to the low column-averaged water vapour content indicated by the Clausius–Clapeyron relation. Given that there are no precipitation observations at elevations above 5300 m, and available evidence suggests that precipitation will likely decrease at high elevations, we scale estimated precipitation using a correction factor p_{cor}:

$$P(Z) = \begin{cases} P(Z), & Z < Z_c \\ P(Z)p_{cor}, & Z_c \le Z < Z_m \\ 0, & Z \ge Z_m \end{cases} \quad (2)$$

where p_{cor} decreases from 1 at the height of a calibrated threshold elevation (Z_c; Table 2) to 0 at Z_m, set here to 7500 m:

$$p_{cor} = 1 - (Z - Z_c)/(Z_m - Z_c). \quad (3)$$

Above 7500 m, we assume that precipitation amounts minus wind erosion and sublimation (Wagnon et al., 2013) are likely to be negligible. The total area above 7500 m represents only 1.2 % of the total basin area.

2.2 Glacier mass balance and redistribution

Following the methods of Immerzeel et al. (2012, 2013), daily accumulation and ablation between 1961 and 2007 are estimated from the gridded T and P fields. All calculations are based on the 90 m SRTM DEM. Daily accumulation is equal to the total

TCD
8, 5375–5432, 2014

precipitation when $T < 0\,^{\circ}\mathrm{C}$, which is a conservative threshold with respect to other studies that have used values of 1.5 or 2 °C (Oerlemans and Fortuin, 1992), but this value has been used in previous Himalayan models (Immerzeel et al., 2012). Daily ablation is estimated using a modified degree day factor (K_c) that varies with DEM-derived aspect (θ) and surface type:

$$K_c = K\left(1 - R_{\mathrm{exp}}\cos\theta\right) \tag{4}$$

where K is the initial melt factor (in $\mathrm{mm}\,^{\circ}\mathrm{C}^{-1}\,\mathrm{d}^{-1}$), and R_{exp} is a factor which quantifies the aspect (or exposure) dependence of K. Initial values for melt factors for snow, ice, and debris covered glaciers (Azam et al., 2014) are given in Table 2. The extent of debris-covered glaciers was extracted from the ICIMOD (2011) glacier inventory.

To redistribute mass from accumulation to ablation areas, we use a simplified flow model which assumes that basal sliding is the principal process for glacier movement, and neglects deformational flow. While cold-based glaciers have been observed on the Tibetan Plateau (Liu et al., 2009), warm-based glaciers and polythermal regimes have been identified on the monsoon-influenced southern slopes of the Himalayas (Mae et al., 1975; Ageta and Higuchi, 1984; Kääb, 2005; Hewitt, 2007). Our assumption in this case is a necessary simplification of the sliding and deformational components of ice flow, that have not yet been modelled at the basin scale in the Himalayas.

Glacier motion is modeled as slow, viscous flow using Weertman's sliding law (Weertman, 1957), which describes glacier movement as a combination of both pressure melting and ice creep near the glacier bed. Glacier flow is assumed to be proportional to the basal shear stress (τ_{b}, Pa):

$$\tau_{\mathrm{b}} \approx v^2 R u^{\frac{2}{n+1}}. \tag{5}$$

Here, v (unitless) is a measure of bedrock roughness, R ($\mathrm{Pa\,m^{-2}\,s}$) is a material roughness coefficient, u is the sliding speed ($\mathrm{m\,s^{-1}}$) and n (unitless) is the creep constant of Glen's flow law, here assumed to equal 3 (Glen, 1955). The roughness of the bedrock

TCD
8, 5375–5432, 2014

(v) is defined as the dimension of objects on the bedrock divided by the distance between them. Smaller values for v indicate more effective regelation. R is a material rougness coefficient that controls the viscous shearing (Fowler, 2010). Basal shear stress (τ_b) is defined as

$$\tau_b = \rho g H \sin\beta \tag{6}$$

where ρ is ice density (kg m^{-3}), g is gravitational acceleration (m s^{-2}), H is ice thickness (m), and β is surface slope (°). We assume that motion occurs only when basal shear stress exceeds the equilibrium shear stress (τ_0 = 80 000 N m^{-2}, Immerzeel et al., 2012), and combine Eqs. (5) and (6) to derive the glacier velocity:

$$u^{\frac{2}{n+1}} = \frac{\max(0, \tau_b - \tau_0)}{v^2 R}. \tag{7}$$

For each time-step, glacier movement in each cell is thus modelled as a function of slope, ice thickness, and assumed bedrock roughness. The total outgoing ice flux at each time step is then determined by the glacier velocity, the horizontal resolution, and the estimated ice depth. This ice volume is apportioned to neighboring downstream cells based on slope, with steeper cells receiving a greater share of the ice flux.

As avalanches can contribute significantly to glacier accumulation in steep mountainous terrain (Inoue, 1977; Scherler et al., 2011), the model incorporates an avalanching component which redistributes accumulated snowfall (Bernhardt and Schulz, 2010). The approach assumes that all snow in a given cell is transported to the downstream cell with the steepest slope whenever snow holding depth and a minimum slope angle is exceeded. The snow holding depth is deep in flat areas and shallow in steep areas and decreases exponentially with increasing slope angle. Based on field observations and an analysis of the slopes of glacierized pixels in the catchment (Fig. 7), we assign a threshold avalanching angle (β_{TH}) of 50°. Change in ice thickness at each time step is thus the net result of ice flow through the cell, ablation, and accumulation from both precipitation and avalanching. Changes in glacier area and volume are calculated at daily

TCD
8, 5375–5432, 2014

timesteps using a 0.2 m w.e. threshold, which represents the average seasonal snowfall depth. The model does not assume steady-state conditions, and reported changes in volume and area thus represent transient states within the model.

2.3 Model initialization and calibration

Initial ice thickness for each glacierized grid cell is calculated as

$$H = \frac{\tau_0}{\rho g \sin\beta}. \quad (8)$$

In the Dudh Kosi basin, Eq. (8) produces a total estimated glacier volume of 32.9 km^3, based on the ICIMOD (2011) glacier inventory and SRTM DEM. While volume-area scaling relations are uncertain (Frey et al., 2013), empirical relations from Huss and Farinotti (2012) and Radić and Hock (2010) applied to individual glaciers generate basin-wide volume estimates of 31.9 and 27.5 km^3, respectively, which lends some support to the approach used here. From the initial ice thicknesses we estimate glacier thicknesses and extents in 1961 by driving the glacier mass balance and redistribution model with modified APHRODITE temperature fields. To simulate the observed climate trends in the region (Shrestha and Aryal, 2011), temperatures in the initialization run are decreased by $-0.025\,^{\circ}C\,yr^{-1}$, for a total decrease of $-1.2\,^{\circ}C$ over the 47 year initialization period. Precipitation is left unchanged in the model initialization, and we use uncalibrated model parameters (Table 2).

From the modelled 1961 ice thicknesses and extents, the model is calibrated with six parameters: degree-day factors for clean ice (ddf_C), debris-covered ice (ddf_I), snow (ddf_S), and debris covered ice on the Khumbu Glacier (ddf_K), material roughness coefficient R, and elevation of the precipitation maximum Z_c (Table 2). Initial simulations showed anomalous flow velocities of the Khumbu glacier which may be due to the assumption that basal sliding is the main process of movement. This may not hold given the steep ice fall above the glacier tongue and the large high altitude accumulation area. We have corrected for this by adopting a specific melt factor for this glacier.

TCD
8, 5375–5432, 2014

Twenty parameter sets were developed by varying the six calibration factors within specified ranges (Table 2). Initial values for each parameter were selected from published studies.

For each of the twenty runs (Table 3), we quantify the model skill by scoring (a) modelled and observed glacier extents at the termini of four large glaciers in the catchment (ICIMOD, 2011), (b) the geodetically-derived mean basin-wide glacier mass balance of $-0.40\,\mathrm{m\,w.e.\,yr^{-1}}$ over the period 1992–2008 (Nuimura et al., 2012), (c) a mean velocity of $10\,\mathrm{m\,yr^{-1}}$ for debris-covered glaciers (Nakawo et al., 1999; Quincey et al., 2009), and (d) the total glacierized area in 2007 ($410\,\mathrm{km^2}$; ICIMOD, 2011). These tests gauge the ability of the model to accurately reproduce key glacier parameters: extent, mass change, and velocity. Scores are derived from the difference between modelled and observed quantities, with a score of zero indicating a perfect match. Scores for all four metrics are multiplied to obtain an overall ranking of the 20 parameter sets, and are weighted equally.

For the glacier extent the score denotes the relative deviation from a perfect match of the four large glaciers around the year 2003 (Fig. 1). For example, if only 20 % of the glacier polygons in Fig. 1 are ice covered then the score equals 0.8. The mass balance score is based on the relative offset from the catchment mean mass balance of $-0.40\,\mathrm{m\,w.e.\,yr^{-1}}$ over the period 1992–2008. If the modelled mean mass balance equals $-0.20\,\mathrm{m\,w.e.\,yr^{-1}}$ then the mass balance score is 0.5. The total ice area score is based on the departure from the total glacierised area at the end of the simulation ($410\,\mathrm{km^2}$, ICIMOD, 2011). If the simulated ice extent is $300\,\mathrm{km^2}$ then the score is 0.27 ((410 – 300)/410). Finally the flow velocity score quantifies the deviation from a mean glacier velocity of debris covered tongues from 1992 to 2008 ($10\,\mathrm{m\,yr^{-1}}$), e.g. if the average simulated flow velocity is $2\,\mathrm{m\,yr^{-1}}$, then the score is 0.8. The final score is a multiplication of the four scores, so in this example the final score is $0.8 \times 0.5 \times 0.27 \times 0.8 = 0.0864$.

TCD
8, 5375–5432, 2014

2.4 Model validation

Temperature and precipitation fields developed for this study were tested independently using point observations of mean daily temperature and total daily precipitation at the four EVK2NCR sites. We calculate mean bias error (MBE) and root mean square error (RMSE) to evaluate the skill of the elevation-based downscaling:

$$\mathrm{MBE} = \frac{1}{n}\sum(\hat{y}_i - y_i) \tag{9}$$

$$\mathrm{RMSE} = \sqrt{\frac{1}{n}\sum(\hat{y}_i - y_i)^2} \tag{10}$$

where n is the number of observations, y_i is the observed value, and $\hat{y}_i$ is the modelled value.

To validate the calibrated glacier mass balance and redistribution model, model outputs are compared against the following independent datasets:

- Ice thickness profiles derived from ground-penetrating radar (GPR) at Mera Glacier (Wagnon et al., 2013) and Changri Nup Glacier (Vincent, unpublished data).
- Annual mass balance and glacier mass balance gradients calculated from surface observations at Mera Glacier (Wagnon et al., 2013)
- Decadal glacier extents (1990, 2000, 2010) extracted from Landsat imagery (Bajracharya et al., 2014a)
- Basin-wide mean annual mass balance from 2000–2011 (Gardelle et al., 2013), and from 1970–2007 (Bolch et al., 2011)

2.5 Climate and glacier change scenarios

To assess the impact of future climate change on glaciers in the Dudh Kosi basin, we drive the calibrated model with the historical climate fields and impose temperature and

TCD
8, 5375–5432, 2014

precipitation changes prescribed from eight CMIP5 climate simulations that represent cold/warm and dry/wet end-members (Table 4; Immerzeel et al., 2013). The prescribed changes are in line with recent downscaling studies conducted in the region (Kulkarni et al., 2013; Dimri and Dash, 2012; Qi et al., 2013). For each model, rates of change in T and P are calculated from the change in mean T and P from 1961–1990 to 2020–2050:

$$\Delta T = \frac{\overline{T}_{2020–2050} - \overline{T}_{1961–1990}}{t - t_0} \quad (11)$$

$$\Delta P = \frac{\overline{P}_{2020–2050} - \overline{P}_{1961–1990}}{t - t_0} \quad (12)$$

where t is equal to 2035, and t_0 is equal to 1975. The linear change rates are then extrapolated to 2100. Uncertainty in our scenarios of future climate change are examined through the mean and SD of modelled ice areas and volumes derived from the eight CMIP5 models. As the model is empirically-based and we assume only changes in T and P (all other state and input variables remain unchanged), we stress that the resulting glacier change estimates should be considered as impact change scenarios as opposed to physically-based projections.

3 Results

3.1 APHRODITE downscaling

Daily vertical temperature gradients calculated from the APHRODITE temperature fields and resampled SRTM range from −0.010 to −0.004 °C m^{-1}, and are highly significant (Fig. 3). Calculated γ_T are most negative in the pre-monsoon (mid-April), and least negative during the active phase of the summer monsoon (mid-June to late August). This is likely a function of the increased moisture advection in the monsoon and pre-monsoon periods, which results in a less negative moist adiabatic lapse

TCD
8, 5375–5432, 2014

rate. These findings are consistent with temperature gradient observations between −0.0046 °C m^{-1} (monsoon) and −0.0064 °C m^{-1} (pre-monsoon) in a nearby Himalayan catchment (Immerzeel et al., 2014b). The SD in calculated γ_T is lowest during the monsoon, and greatest in the winter.

At all four EVK2CNR stations, daily temperatures estimated from APHRODITE vertical gradients are greater than observed, with mean daily differences ranging from −1 to +8 °C (Fig. 4). Micro-meteorological conditions may contribute to the larger biases observed at Pyramide (winter) and Pheriche (summer). During the summer monsoon period (mid-June to mid-September), the mean difference for all stations is approximately 5 °C. We develop a bias correction for the day of year (DOY) based on the mean temperature bias from the four stations, which ranges from 3.22 to 6.00 °C. The largest bias coincides with the approximate onset of the summer monsoon (DOY 150, or 31 May). A possible mechanism for this is the pre-monsoon increase in humidity at lower elevations, which would be well-represented in the gridded APHRODITE data, but not at the higher elevation EVK2CNR stations. The increased humidity would result in a less negative derived temperature gradient, and thus greater errors at the high-elevation stations. The variability in calculated temperature gradients is sharply reduced at onset of the monsoon, which supports this hypothesis. Bias-corrected estimates of daily temperature (Fig. 8) have root mean squared errors (RMSE) of 1.21 to 2.07 °C, and mean bias errors (MBE) of −0.87 to 0.63 °C.

Daily precipitation-elevation functions (Fig. 5) exhibit strong decreases in precipitation above 4000 m, particularly in the monsoon and pre-monsoon periods. Absolute precipitation totals are greatest during the monsoon period, but large precipitation events can still occur in the post-monsoon period (October–November). As often observed in high-elevation environments, daily precipitation totals observed at the EVK2CNR stations are not well captured by the downscaling process (Fig. 6). This is likely due to the difficulties in estimating precipitation in complex terrain (Immerzeel et al., 2012; Pellicciotti et al., 2012), and to errors in the precipitation measurements. For daily liquid precipitation ($T > 0$), RMSE range between 2.05 and 8.21 mm, while

TCD
8, 5375–5432, 2014

MBE range from −0.85 to 1.77 mm. However, accumulated precipitation totals (Fig. 6) and mean monthly precipitation values show greater coherence, which lends some support for the downscaling approach used. At Pyramid (5035 m), the highest station with precipitation observations, the fit between cumulative modelled and observed precipitation is quite close. However, at Pheriche (4260 m), modelled precipitation is nearly double that observed over the period of record, which suggests that further refinements to the precipitation downscaling method are needed.

3.2 Model results and validation

For the calibration runs, we report here volume and area values averaged between 1 November and 31 January. Reported uncertainties are the SD in modelled values from the 20 simulations. Modelled ice volumes from the 20 calibration runs (Fig. 9) decrease from 41.0 km^3 in 1961 to between 31.6 and 37.1 km^3 in 2007, with a 20-member mean of 34.5 ± 1.5 km^3 at the end of the simulation period. The ensemble mean modelled glacierized area in the calibration runs decreases from 499 to 392 ± 11 km^2, with a final range of 374 to 397 km^2.

Parameters for the calibrated model were chosen based on the scores of the 20 parameter sets (Table 3). Four model runs (5, 10, 15, and 17) had low overall scores (< 0.0001), and we select the parameters from Run 5 on the basis of its improved performance with respect to basin-wide mass balance and glacier velocities. Simulations from model 5 generate glacier volume and area totals that are lower than the multi-model mean (Fig. 9), but are within the SD of the models. The final calibrated degree-day factors (Table 2) are all slightly higher than those observed by Azam et al. (2014) at Chhota Shigri Glacier, but are similar to values obtained for snow and ice by Singh et al. (2000) at Dokriani Glacier, Garwhal Himalaya. The calibrated value for the material roughness coefficient lies between the values used previously in Baltoro (Pakistan) and Langtang (Nepal, Fig. 1) catchments (Immerzeel et al., 2013, Supplement).

Spatially distributed output from the calibrated model (Run 5), 1961–2007, is summarized in Fig. 10. Mean annual ablation (Fig. 10a) ranges from 0 to 4.00 m w.e. yr^{-1},

TCD
8, 5375–5432, 2014

though most modelled values are less than 1.80 m w.e. yr^{-1}. Debris-covered termini, despite having lower degree day factors, are nevertheless subjected to large melt rates due to their relatively low elevation and consequently higher temperatures. Our model generates maximum melt rates at the transition between debris-covered and clean glacier ice, at elevations of approximately 5000 m (Fig. 2). This is consistent with geodetic observations of mass change in the catchment (e.g. Bolch et al., 2008b). Maximum mean annual snowfall (Fig. 10b) amounts of up to 0.50 m w.e. yr^{-1} are observed at 6268 m (the calibrated value of Z_c, Table 2), but due to the precipitation scaling function (Eq. 2) the highest peaks receive zero snowfall amounts. The calibrated height of Z_c (6268 m) is similar to the elevation of maximum snowfall (between 6200 and 6300 m) estimated for the Annapurna range in mid-Nepal (Fig. 1; Harper and Humphrey, 2003).

Over the entire domain, modelled mean annual mass balances (Fig. 10c) range from −4.6 to +3.0 m w.e. yr^{-1}, with the majority of values falling between −1.4 and +0.1 m w.e. yr^{-1}. The spatial patterns of modelled annual mass balance are consistent with the geodetic estimates of mass change between 2000 and 2010, and our modelled basin-wide mass balance of −0.33 m w.e. yr^{-1} is only slightly more negative than the basin-wide estimates of -0.26 ± 0.13 m w.e. yr^{-1} given by Gardelle et al. (2013), and -0.27 ± 0.08 m w.e. yr^{-1} given by Bolch et al. (2011) for the Khumbu reigon only. The overall Dudh Kosi mass balance gradient, calculated from median modelled b_a for all glacierized cells between 4850 and 5650 m, is equivalent to 0.27 m w.e. (100 m)$^{-1}$ (Fig. 11). With this mass balance gradient, we calculate a basin-wide ELA at approximately 5500 m, which agrees with previously published estimates (Williams, 1983; Asahi, 2010; Wagnon et al., 2013). Extracting the grid cells for Mera Glacier only, we calculate a mass balance gradient of approximately 0.40 m w.e. (100 m)$^{-1}$ between 5350 and 5600 m, which compares well with the gradient of 0.48 m w.e (100 m)$^{-1}$ observed over the same elevation range at Mera Glacier between 2007 and 2012 (Wagnon et al., 2013).

Modelled mass balances at Mera Glacier (1961–2007) range between −1.45 and +0.11 m w.e. (Fig. 12), while surface mass balance observations at the same site from

TCD
8, 5375–5432, 2014

2007 to 2012 range between −0.67 and +0.46 m w.e. (Wagnon et al., 2013). As model and observation periods do not overlap, direct comparisons between modelled and observed mass balances are not possible. However, the mean mass balance observed at Mera Glacier between 2007 and 2012 is −0.08 m w.e., whereas the mean modelled mass balance between 2000 and 2006 is −0.16 m w.e. We note that our reconstructed mass balance series at Mera Glacier shows strong similarities to the reconstructed mass balance at Chhota Shigri Glacier (Azam et al., 2014), with balanced conditions in the late 1980s and early 1990s. Standard deviations of observed and modelled mass balance are 0.51 and 0.29 m w.e., respectively, and the greater variability in observed b_a is likely linked to the short observation period (5 year) and to enhanced local variability which cannot be captured with downscaled climate fields. The mass balance model, although it may underestimate the inter-annual variability, is able to simulate a surface mass balance which is in a plausible and realistic range.

3.3 Modelled and observed glacier thickness

At the end of the calibrated run (1961–2007), modelled ice thicknesses range between 0 and 620 m, though 98 % of these are less than 205 m (Fig. 10d). Similar ice thicknesses have been estimated for the large debris-covered Gangotri Glacier, Indian Himalaya, using slope, surface velocities, and simple flow laws (Gantayat et al., 2014). Due to the model formulation, low-angle slopes on glacier termini may result in unrealistic estimates of ice depth, and a minimum surface slope of 1.5° is prescribed in the model. Radio-echo surveys in 1999 indicated that centerline ice thicknesses on the Khumbu Glacier decreased from approximately 400 m at Base Camp to less than 100 m near the terminus (Gades et al., 2000). Our model accurately captures this decrease in the upper portions, but overestimates ice thickness in the relatively flat terminus. Recent observations of ice thickness obtained from ground penetrating radar (GPR) surveys in the basin are examined in detail below.

Estimates of glacier thickness extracted from the calibrated model are compared with depth profiles found with GPR surveys conducted at Mera Glacier (Wagnon et al.,

TCD
8, 5375–5432, 2014

2013) and Changri Nup Glacier (C. Vincent, unpublished data). To facilitate the comparison, we obtained surface elevations and bedrock depths from the GPR surveys, and we matched these to the modeled ice thicknesses of the corresponding pixels (Fig. 13). At the lower elevation profile on Mera Glacier (5350 m), the shape of the bedrock profile is similar to the model, but ice thicknesses are approximately half what is observed or less. This may be due in part to the surface slope extracted from the DEM, which controls the modelled ice thickness. The transect at 5350 m was collected in a flat section between two steeper slopes, which would likely be mapped as a steep slope in the DEM. For the profile at 5520 m both the shape and the depths of the bedrock profile are generally well-captured by the model. At the Changri Nup cross section, which lies on a relatively flat section of the main glacier body, modelled ice depths are approximately 2/3 of the observed.

3.4 Modelled and observed glacier shrinkage

Modelled historical changes in glacier area (Fig. 9) exhibit greater variability than modelled ice volumes. This is largely due to the sensitivity of the modelled glacier area to large snowfall events, as pixels with a snow water equivalent above 0.2 m w.e. threshold are classified as glacier. To compare modelled and observed extents we use the mean extent at the end of the ablation season (1 November–31 January).

Using semi-automated classifications of Landsat imagery (ICIMOD, 2011; Bajracharya et al., 2014b), glacier extents in the Dudh Kosi basin were constructed for 1990, 2000, and 2010. As the glacier change signal is greatest at lower elevations, and errors in glacier delineation due to persistent snow cover are possible at higher elevations, we consider the change in glacier area below 5500 m, which roughly equals the equilibrium line altitude in the catchment.

Below 5500 m, the total change in glacier area in the Dudh Kosi was $-0.61\,\%\,yr^{-1}$ between 1990 and 2000, and $-0.79\,\%\,yr^{-1}$ between 2000 and 2010. Modelled rates of glacier area change below 5500 m are $-0.36\,\%\,yr^{-1}$ (1990–2000) and $-0.71\,\%\,yr^{-1}$ (2000–2007). Both modelled and observed glacier change are of similar magnitudes,

TCD
8, 5375–5432, 2014

and both show a consistent trend of increasing area loss, which is corroborated by other studies in the region (Bolch et al., 2008b; Thakuri et al., 2014). Differences between modelled and observed rates of glacier shrinkage can be attributed to both errors in the glacier inventory, e.g. geometric correction and interpretation errors, and model shortcomings.

3.5 Glacier change scenarios

Temperature and precipitation trends extracted from CMIP5 end members (Table 4) are applied to the historical APHRODITE *T* and *P* fields, and the calibrated glacier mass and redistribution model is used to explore possible future glacier changes in the Dudh Kosi basin. From initial glacier volumes and extents (Eq. 8), the mean projected changes in total ice volume at 2050 are −45 and −52 % for RCP4.5 and RCP8.5 emissions scenarios, respectively (Table 5). The minimum projected volume change at 2050 is −35 % (cold/wet), and the maximum is −62 % (warm/dry). At 2100 the projected mean total volume loss is estimated at −83 % for RCP4.5 scenarios, and −89 % for RCP8.5, with a range between −73 and −96 %. Radić et al. (2014) and Marzeion et al. (2012), respectively, estimate mean glacier volume changes in south-east Asia of −50 and −60 % for RCP4.5 scenarios, and −75 and −70 % for RCP8.5 by 2100. In all scenarios presented here, the rate of ice loss decreases towards the end of the simulation period (Fig. 14), which indicates a shift towards equilibrium mass balance conditions.

The greatest impact on future glacier mass change occurs under scenarios of warm and dry future conditions (Fig. 14, Table 4). However, the mass change under warm/dry and warm/wet scenarios for RCP4.5 are nearly identical. This indicates that the future impacts on glaciers in the region are more dependent on the temperature change signal than on any changes in precipitation. Changes in the timing and magnitude of monsoon precipitation may thus be less important than previously believed (Mölg et al., 2012; Bolch et al., 2012). The main difference between the RCP4.5 and RCP8.5 scenarios is

TCD
8, 5375–5432, 2014

the magnitude of the temperature increase, which leads to greater losses of ice volume in the RCP8.5 scenarios.

With a distributed model we can investigate the possible impact of future climate change on Everest-region glacier area and thickness with respect to elevation. The patterns of decreases in ice area (Fig. 15) and ice thickness (Fig. 16) with elevation illustrate the combined effects of increased melt rates due to warmer temperatures and the insulating effect of debris cover. The greatest losses in glacier area, both relative and absolute, are expected at elevations close to the current ELA (approx. 5500 m), where the greatest amount of glacierized area currently exists. At lower elevations, where glaciers are exclusively debris-covered (Fig. 2), modelled glacier thicknesses are greater (Fig. 10), and response times are slower, modelled changes in glacier area and volume will be less than those near the ELA. Above 6000 m, future changes in glacierized area are also expected to be small.

Wet and cool scenarios for both the RCP4.5 and RCP8.5 scenarios show the possible survival of debris covered glaciers between 4000 and 4500 m, albeit with greatly reduced thicknesses. In both warm and dry scenarios, glaciers below 5500 m could be eliminated, and in the RCP8.5 scenario, glacier thicknesses between 6000 and 6500 m could experience reductions by the year 2100. According to these scenarios, no changes are expected in the glacier volumes at elevations above 7000 m.

The RCP8.5 warm/dry scenario is the worst-case projection, in which the area of glaciers between 4500 and 6200 m is reduced by more than 80 % by 2100 (Fig. 15c). The projected rate of temperature increase (3.1 °C by 2050; Immerzeel et al., 2013) is strong enough to cause reductions in glacierized area at all elevations by 2100. Under the RCP4.5 scenario of reduced warming and increased precipitation (Fig. 15b), the glacierized area near the ELA is still expected to decline by nearly 80 %, with reductions of only 40 % on debris-covered portions by 2100.

TCD
8, 5375–5432, 2014

4 Discussion

Through a multi-parameter calibration and validation with independent datasets, we model the mass balance and mass redistribution of glaciers in the Dudh Kosi basin over the period 1961–2007, and use projected temperature and precipitation changes from the CMIP5 ensembles to create an envelope of possible future glacier responses. While we have provided broad estimates of model uncertainty with 20 historical runs from randomly sampled parameters, a full accounting of model uncertainty and parameter sensitivity has yet to be conducted. Although considerable progress is made by the systematic integration of field based observations into our modelling approach, there are still a number of key challenges to be addressed in the future.

The lack of high elevation temperature and precipitation data to force the mass balance model is one of the key challenges that nearly all Himalayan modelling studies face. In this study, we derive temperature gradients and precipitation-elevation functions from the 0.25° gridded APHRODITE data, which in turn is based primarily on low-elevation stations. The downscaling approach is then tested with independent station data from the EVK2CNR network of stations in the Dudh Kosi basin. While we obtain highly significant matches with daily temperatures after applying a bias-correction based on the day of year, our ability to model precipitation ranges from very good (at Pyramid) to very poor (at Pheriche). Difficulty in quantifying precipitation and precipitation gradients in high-mountain areas is likely one of the largest sources of uncertainty in mountain hydrology (Immerzeel et al., 2012; Nepal et al., 2014). The absence of dense observation networks in the Himalayas limits the ability to use geostatistical or interpolation tools (e.g. Daly et al., 1994). It is worth noting that the elevation-based approach used here matches the two-step precipitation patterns found from the TRMM observations (Bookhagen and Burbank, 2006; Shrestha et al., 2012), and the reduction in precipitation up to 5000 m. Further investigations into high-elevation precipitation gradients, through field studies, remote sensing derivatives, and/or the use of high-resolution numerical weather models, will help to increase our understanding of

TCD
8, 5375–5432, 2014

glacier nourishment in the region. A sensitivity analysis of modelled glacier change to the rain/snow threshold temperature is also recommended.

The glacier mass balance and redistribution model used in this study has precedents in other studies (Immerzeel et al., 2012, 2013). However, a critical component of the current study is the calibration we perform with observational data, and our use of available field and remotely sensed observations to test the model qualitatively and to constrain key model parameters such as the sliding threshold. We have demonstrated that the mass balance and redistribution model, though relatively simple, is able to represent the regional patterns of mass and area change over time, which lends some confidence for the future projections. As 25 % of the glacierized area is debris-covered (Fig. 2), there are significant uncertainties with respect to both melt rates under debris-covered glaciers (Nicholson and Benn, 2006) and the effects of debris-cover on glacier dynamics (Naito et al., 2000). Until higher-order models of Himalayan glacier dynamics (e.g. Adhikari and Huybrechts, 2009) are sufficently advanced and explicitly include the effects of debris cover, and the additional input data (bedrock topography, ice temperatures) and are well-constrained, simple modelling approaches will still be required for basin-scale analyses of glacier change scenarios.

Two further limitations of our study are the assumptions that CMIP5 T and P changes are linear with respect to elevation and that the downscaled climate fields are stationary. Changes in T and P were calculated from the 1961–1990 baseline to 2021–2050, and we extrapolate these values out to the year 2100, while the response of the climate system is not likely to be linear. One advantage to using the delta approach (where temperature and precipitation changes are applied to historical climate data) is that the natural temporal variability in the climate system is retained. There is some suggestion that amplification of the summer monsoon will occur in the future (Lee and Wang, 2014). This may result in increased accumulation at higher elevations, but will also be accompanied by an upwards shift in the snowline elevation. Significant snowfall events during the monsoon may slow the loss of ice from lower ablation zones, but with increasing temperatures such events will occur less frequently. Given that the

TCD
8, 5375–5432, 2014

capability of climate models to simulate the present day monsoon, let alone future monsoon shifts, is quite poor (Turner and Annamalai, 2012), we consider the assumption of linearity in climate change signal acceptable. All future scenarios suggest that the impact of climate change will be strongly negative, and our results are indicative of the glacier sensitivity within plausible future bounds.

Our modelled results indicate that glaciers in the region are highly sensitive to temperature changes. Precipitation increases of 15 % (mostly during the monsoon season) will be unable to counter the loss of glacier mass due to increased melt rates. Under warm and dry conditions from the RCP8.5 ensembles, glacier volumes in the Dudh Kosi at the end of the century are projected to be only 5 % of their current volumes, and our ensemble mean volume change is more negative than regional estimates given by both Marzeion et al. (2012) and Radić et al. (2014). The actual response times of glaciers in the region can be approximated from the modelled thicknesses and accumulation rates near the glacier terminus, following the methods of Jóhannesson et al. (1989):

$$\tau = \frac{-H'}{\dot{b}_t} \tag{13}$$

where H' is a representative glacier thickness and $\dot{b}_a$ ($\dot{b}_a > 0$) is the mean annual mass balance near the terminus. Given our modeled ice thicknesses and mean annual mass balances at the termini of glaciers throughout the catchment, Eq. (13) suggests that the smaller glaciers in the southern portions of the basin have total glacier response times on the order of 20–50 year, while the large debris-covered glaciers have response times of 200–500 year. These first-order estimates reflect the time it takes the glaciers to reach a new equilibrium state in response to a step change in climate (Cogley et al., 2011), and are in agreement with the modelled persistence of debris-covered termini.

Our scenarios suggest that future reductions in glacier area will occur mainly in clean ice regions between accumulation areas and debris-covered termini. We anticipate that the hypsometric distribution of ice will become bi-modal as glacier mass loss proceeds: debris-covered tongues will continue to exist (in reduced states) at low elevations, but

TCD
8, 5375–5432, 2014

will become separated from their high-elevation accumulation zones (Kääb, 2005). Current examples of this type of glacier change can be found at Chorabari Glacier, Garwhal Himalaya (Dobhal et al., 2013) and at Lirung Glacier (central Nepal) in nearby Langtang Valley (Immerzeel et al., 2014a), where glacier wastage above the debris-covered termini has left stagnant debris-covered ice below and small high-elevation ice masses above. Model scenarios from this study are thus consistent with field observations, and suggest that this will become a familiar picture in the coming decades.

5 Conclusions

In the mountains of high Asia, changes in glacier volumes will impact the timing and magnitude of streamflows, particularly in the pre-monsoon period (Immerzeel et al., 2013). Our study advances the current understanding of Himalayan glacier evolution under climate change, and examines the basin-scale evolution of glaciers in the Dudh Kosi basin of central Nepal using a distributed glacier mass balance and redistribution model. We constrain the glacier model parameters with observations where possible, and calibrate against observations of net glacier mass change, velocities on debris-covered termini, and glacier extents. Our work represents a first-order estimate of future glacier change scenarios, that should be improved in the future with a more physically-based representation of ice dynamics.

End-member scenarios of future climate change in the region, extracted from CMIP5 RCP4.5 and RCP8.5 ensembles (Immerzeel et al., 2013), are applied linearly to historical downscaled climate fields, and the model is used to explore scenarios of future climate change on glaciers in the Dudh Kosi basin. We project decreases in ice volumes, relative to those estimated for 2007, of between −35 and −62 % by 2050, and decreases of between −73 and −96 % by 2100, assuming a constant linear change in temperature and precipitation. The majority of the mass wastage occurs between elevations of 5000 and 6000 m, where significant areas of clean ice currently exist.

TCD
8, 5375–5432, 2014

Glaciers in the region are highly sensitive to changes in temperature, and projected increases in precipitation are insufficient to offset the increased melt that will accompany higher temperatures and an increased ELA. Future research on high-altitude precipitation gradients and increased field observations for model calibration and testing will help reduce the uncertainty in our estimates of strongly negative future glacier mass and area change in the Everest region, and our scenarios of glacier change will be linked with hydrological models (Nepal et al., 2014; Immerzeel et al., 2013) to investigate possible future changes in the timing and magnitude of streamflows.

Acknowledgements. We gratefully acknowledge the Royal Norwegian Embassy at Kathmandu for funding the Cryosphere Monitoring Project at the ICIMOD, and the contributions of Finu Shrestha and Sudan Maharajan to the glacier inventory work. This study was partially funded by the Netherlands Organization for Scientific Research through their VENI program and by the research for development (R4D) program of DFID, as well as core funds of ICIMOD contributed by the governments of Afghanistan, Australia, Austria, Bangladesh, Bhutan, China, India, Myanmar, Nepal, Norway, Pakistan, Switzerland, and the UK. Mera and Changri Nup glacier research was supported by the French Service d'Observation GLACIOCLIM and the French National Research Agency through ANR-09-CEP-005-01/PAPRIKA. This study was carried out within the framework of the Ev-K2-CNR Project in collaboration with the Nepal Academy of Science and Technology as foreseen by the Memorandum of Understanding between Nepal and Italy, and thanks to contributions from the Italian National Research Council, the Italian Ministry of Education, University and Research, and the Italian Ministry of Foreign Affairs. We also acknowledge the World Climate Research Programme's Working Group on Coupled Modelling, which is responsible for CMIP, and we thank the climate modelling groups for producing and making available their model outputs. The views and interpretations in this publication are those of the authors and are not necessarily attributable to ICIMOD. Anne Rowan, Graham Cogley, and an anonymous reviewer provided invaluable comments and suggestions on previous versions of this manuscript.

TCD
8, 5375–5432, 2014

References

Adhikari, S. and Huybrechts, P.: Numerical modelling of historical front variations and the 21st-century evolution of glacier AX010, Nepal Himalaya, Ann. Glaciol., 50, 27–34, 2009. 5398

Ageta, Y. and Higuchi, K.: Estimation of mass balance components of a summer-accumulation type glacier in the Nepal Himalaya, Geogr. Ann. A, 66, 249–255, 1984. 5380, 5384

Ageta, Y. and Kadota, T.: Predictions of changes of glacier mass balance in the Nepal Himalaya and Tibetan Plateau: a case study of air temperature increase for three glaciers, Ann. Glaciol., 16, 89–94, 1992. 5380

Asahi, K.: Equilibrium-line altitudes of the present and Last Glacial Maximum in the eastern Nepal Himalayas and their implications for SW monsoon climate, Quatern. Int., 212, 26–34, doi:10.1016/j.quaint.2008.08.004, 2010. 5379, 5392

Ashfaq, M., Shi, Y., Tung, W.-W., Trapp, R. J., Gao, X., Pal, J. S., and Diffenbaugh, N. S.: Suppression of south Asian summer monsoon precipitation in the 21st century, Geophys. Res. Lett., 36, L01704, doi:10.1029/2008GL036500, 2009. 5380

Azam, M. F., Wagnon, P., Vincent, C., Ramanathan, A., Linda, A., and Singh, V. B.: Reconstruction of the annual mass balance of Chhota Shigri glacier, Western Himalaya, India, since 1969, Ann. Glaciol., 55, 69–80, doi:10.3189/2014AoG66A104, 2014. 5384, 5391, 5393

Bajracharya, S. R. and Mool, P.: Glaciers, glacial lakes and glacial lake outburst floods in the Mount Everest region, Nepal, Ann. Glaciol., 50, 81–86, doi:10.3189/172756410790595895, 2010. 5378

Bajracharya, S. R., Maharjan, S., Shrestha, F., Bajracharya, O., and Baidya, S.: Glacier Status in Nepal and Decadal Change from 1980 to 2010 Based on Landsat Data, ICIMOD, available at: lib.icimod.org/record/29291 (last access: 29 August 2014), 2014a. 5388

Bajracharya, S. R., Maharjan, S. B., and Shrestha, F.: The status and decadal change of glaciers in Bhutan from the 1980s to 2010 based on satellite data, Ann. Glaciol., 55, 159–166, doi:10.3189/2014AoG66A125, 2014b. 5394

Benn, D. I., Bolch, T., Hands, K., Gulley, J., Luckman, A., Nicholson, L. I., Quincey, D., Thompson, S., Toumi, R., and Wiseman, S.: Response of debris-covered glaciers in the Mount Everest region to recent warming, and implications for outburst flood hazards, Earth-Sci. Rev., 114, 156–174, doi:10.1016/j.earscirev.2012.03.008, 2012. 5378

Bernhardt, M. and Schulz, K.: SnowSlide: a simple routine for calculating gravitational snow transport, Geophys. Res. Lett., 37, L11502, doi:10.1029/2010GL043086, 2010. 5385

TCD
8, 5375–5432, 2014

Bolch, T., Buchroithner, M., Pieczonka, T., and Kunert, A.: Planimetric and volumetric glacier changes in the Khumbu Himal, Nepal, since 1962 using Corona, Landsat TM and ASTER data, J. Glaciol., 54, 592–600, doi:10.3189/002214308786570782, 2008a. 5378

Bolch, T., Buchroithner, M. F., Peters, J., Baessler, M., and Bajracharya, S.: Identification of glacier motion and potentially dangerous glacial lakes in the Mt. Everest region/Nepal using spaceborne imagery, Nat. Hazards Earth Syst. Sci., 8, 1329–1340, doi:10.5194/nhess-8-1329-2008, 2008b. 5378, 5392, 5395

Bolch, T., Pieczonka, T., and Benn, D. I.: Multi-decadal mass loss of glaciers in the Everest area (Nepal Himalaya) derived from stereo imagery, The Cryosphere, 5, 349–358, doi:10.5194/tc-5-349-2011, 2011. 5388, 5392

Bolch, T., Kulkarni, A., Kääb, A., Huggel, C., Paul, F., Cogley, J. G., Frey, H., Kargel, J. S., Fujita, K., Scheel, M., Bajracharya, S., and Stoffel, M.: The state and fate of Himalayan glaciers, Science, 336, 310–314, doi:10.1126/science.1215828, 2012. 5378, 5379, 5395

Bookhagen, B. and Burbank, D.: Topography, relief, and TRMM-derived rainfall variations along the Himalaya, Geophys. Res. Lett., 33, L08405, doi:10.1029/2006GL026037, 2006. 5378, 5397

Bookhagen, B. and Burbank, D. W.: Toward a complete Himalayan hydrological budget: spatiotemporal distribution of snowmelt and rainfall and their impact on river discharge, J. Geophys. Res.-Earth, 115, F03019, doi:10.1029/2009JF001426, 2010. 5378

Chen, N. Sh., Hu, G. Sh., Deng, W., Khanal, N., Zhu, Y. H., and Han, D.: On the water hazards in the trans-boundary Kosi River basin, Nat. Hazards Earth Syst. Sci., 13, 795–808, doi:10.5194/nhess-13-795-2013, 2013. 5378

Cogley, J. G.: Present and future states of Himalaya and Karakoram glaciers, Ann. Glaciol., 52, 69–73, doi:10.3189/172756411799096277, 2011. 5380

Cogley, J. G., Hock, R., Rasmussen, L., Arendt, A., Bauder, A., Braithwaite, R., Jansson, P., Kaser, G., Möller, M., Nicholson, L., and Zemp, M.: Glossary of glacier mass balance and related terms. IHP-VII Technical Documents in Hydrology No. 86, IACS Contribution No. 2, UNESCO-IHP, Paris, 126 pp., 2011. 5399

Daly, C., Neilson, R. P., and Phillips, D. L.: A statistical-topographic model for mapping climatological precipitation over mountainous terrain, J. Appl. Meteorol., 33, 140–158, 1994. 5397

Dimri, A. and Dash, S.: Wintertime climatic trends in the western Himalayas, Climatic Change, 111, 775–800, doi:10.1007/s10584-011-0201-y, 2012. 5380, 5389

TCD
8, 5375–5432, 2014

Dimri, A., Yasunari, T., Wiltshire, A., Kumar, P., Mathison, C., Ridley, J., and Jacob, D.: Application of regional climate models to the Indian winter monsoon over the western Himalayas, Sci. Total Environ., 468, S36–S47, doi:10.1016/j.scitotenv.2013.01.040, 2013. 5381

Dobhal, D., Mehta, M., and Srivastava, D.: Influence of debris cover on terminus retreat and mass changes of Chorabari Glacier, Garhwal region, central Himalaya, India, J. Glaciol., 59, 961, doi:10.3189/2013JoG12J180, 2013. 5400

Farr, T. G., Rosen, P. A., Caro, E., Crippen, R., Duren, R., Hensley, S., Kobrick, M., Paller, M., Rodriguez, E., Roth, L., Seal, D., Shaffer, S., Shimada, J., Umland, J., Werner, M., Oskin, M., Burbank, D., and Alsdorf, D.: The shuttle radar topography mission, Rev. Geophys., 45, RG2004, doi:10.1029/2005RG000183, 2007. 5382

Fowler, A. C.: Weertman, Lliboutry and the development of sliding theory, J. Glaciol., 56, 965–972, doi:10.3189/002214311796406112, 2010. 5385

Frey, H., Machguth, H., Huss, M., Huggel, C., Bajracharya, S., Bolch, T., Kulkarni, A., Linsbauer, A., Salzmann, N., and Stoffel, M.: Ice volume estimates for the Himalaya–Karakoram region: evaluating different methods, The Cryosphere Discuss., 7, 4813–4854, doi:10.5194/tcd-7-4813-2013, 2013. 5386

Fujita, K. and Nuimura, T.: Spatially heterogeneous wastage of Himalayan glaciers, P. Natl. Acad. Sci. USA, 108, 14011–14014, doi:10.1073/pnas.1106242108, 2011. 5380

Gades, A., Conway, H., Nereson, N., Naito, N., and Kadota, T.: Radio echo-sounding through supraglacial debris on Lirung and Khumbu Glaciers, Nepal Himalayas, in: Proceedings of International Workshop on Debris Covered Glaciers, IAHS-AISH Publ., 264, 13–22, 2000. 5393

Gantayat, P., Kulkarni, A., and Srinivasan, J.: Estimation of ice thickness using surface velocities and slope: case study at Gangotri Glacier, India, J. Glaciol., 60, 277–282, doi:10.3189/2014JoG13J078, 2014. 5393

Gardelle, J., Berthier, E., and Arnaud, Y.: Slight mass gain of Karakoram glaciers in the early twenty-first century, Nat. Geosci., 5, 322–325, doi:10.1038/ngeo1450, 2012. 5378

Gardelle, J., Berthier, E., Arnaud, Y., and Kääb, A.: Region-wide glacier mass balances over the Pamir-Karakoram-Himalaya during 1999–2011, The Cryosphere, 7, 1263–1286, doi:10.5194/tc-7-1263-2013, 2013. 5378, 5388, 5392

TCD
8, 5375–5432, 2014

Gardner, A. S., Moholdt, G., Cogley, J. G., Wouters, B., Arendt, A. A., Wahr, J., Berthier, E., Hock, R., Pfeffer, W. T., Kaser, G., Ligtenberg, S. R. M., Bolch, T., Sharp, M. J., Hagen, J. O., van den Broeke, M. R., and Paul, F.: A reconciled estimate of glacier contributions to sea level rise: 2003 to 2009, Science, 340, 852–857, doi:10.1126/science.1234532, 2013. 5378

Gautam, M. R., Acharya, K., and Tuladhar, M. K.: Upward trend of streamflow and precipitation in a small, non-snow-fed, mountainous watershed in Nepal, J. Hydrol., 387, 304–311, 2010. 5380

Glen, J. W.: The creep of polycrystalline ice, P. R. Soc. Lond. A, 228, 519–538, doi:10.1098/rspa.1955.0066, 1955. 5384

Harper, J. T. and Humphrey, N. F.: High altitude Himalayan climate inferred from glacial ice flux, Geophys. Res. Lett., 30, 1764, doi:10.1029/2003GL017329, 2003. 5383, 5392

Hewitt, K.: Tributary glacier surges: an exceptional concentration at Panmah Glacier, Karakoram Himalaya, J. Glaciol., 53, 181–188, doi:10.3189/172756507782202829, 2007. 5384

Huss, M. and Farinotti, D.: Distributed ice thickness and volume of all glaciers around the globe, J. Geophys. Res.-Earth, 117, F04010, doi:10.1029/2012JF002523, 2012. 5386

ICIMOD: The Status of Glaciers in the Hindu Kush-Himalayan Region, ICIMOD, Kathmandu, 2011. 5377, 5384, 5386, 5387, 5394, 5414, 5417, 5418, 5423

Immerzeel, W. W., van Beek, L. P. H., and Bierkens, M. F. P.: Climate change will affect the Asian water towers, Science, 328, 1382–1385, doi:10.1126/science.1183188, 2010. 5376, 5377, 5413

Immerzeel, W. W., van Beek, L., Konz, M., Shrestha, A., and Bierkens, M.: Hydrological response to climate change in a glacierized catchment in the Himalayas, Climatic Change, 110, 721–736, doi:10.1007/s10584-011-0143-4, 2012. 5380, 5383, 5384, 5385, 5390, 5397, 5398

Immerzeel, W. W., Pellicciotti, F., and Bierkens, M.: Rising river flows throughout the twenty-first century in two Himalayan glacierized watersheds, Nat. Geosci., 6, 742–745, doi:10.1038/ngeo1896, 2013. 5377, 5380, 5383, 5389, 5391, 5396, 5398, 5400, 5401, 5415

Immerzeel, W. W., Kraaijenbrink, P., Shea, J., Shrestha, A., Pellicciotti, F., Bierkens, M., and de Jong, S.: High-resolution monitoring of Himalayan glacier dynamics using unmanned aerial vehicles, Remote Sens. Environ., 150, 93–103, 2014a. 5400

TCD
8, 5375–5432, 2014

Immerzeel, W. W., Petersen, L., Ragettli, S., and Pellicciotti, F.: The importance of observed gradients of air temperature and precipitation for modeling runoff from a glacierized watershed in the Nepalese Himalayas, Water Resour. Res., 50, 2212–2226, doi:10.1002/2013WR014506, 2014b. 5390

Inoue, J.: Mass budget of Khumbu Glacier: glaciological expedition of Nepal, Contribution No. 32, Seppyo, 39, 15–19, 1977. 5385

Jacob, T., Wahr, J., Pfeffer, W., and Swenson, S.: Recent contributions of glaciers and ice caps to sea level rise, Nature, 482, 514–518, doi:10.1038/nature10847, 2012. 5378

Jóhannesson, T., Raymond, C., and Waddington, E.: Time-scale for adjustment of glaciers to changes in mass balance, J. Glaciol., 35, 355–369, 1989. 5399

Kääb, A.: Combination of SRTM3 and repeat ASTER data for deriving alpine glacier flow velocities in the Bhutan Himalaya, Remote Sens. Environ., 94, 463–474, 2005. 5384, 5400

Kääb, A., Berthier, E., Nuth, C., Gardelle, J., and Arnaud, Y.: Contrasting patterns of early twenty-first-century glacier mass change in the Himalayas, Nature, 488, 495–498, doi:10.1038/nature11324, 2012. 5378

Kripalani, R. H., Oh, J. H., Kulkarni, A., Sabade, S. S., and Chaudhari, H. S.: South Asian summer monsoon precipitation variability: coupled climate model simulations and projections under IPCC AR4, Theor. Appl. Climatol., 90, 133–159, doi:10.1007/s00704-006-0282-0, 2007. 5380

Kulkarni, A., Patwardhan, S., Kumar, K. K., Ashok, K., and Krishnan, R.: Projected climate change in the Hindu Kush-Himalayan region by using the high-resolution regional climate model PRECIS, Mt. Res. Dev., 33, 142–151, 2013. 5389

Lee, J.-Y. and Wang, B.: Future change of global monsoon in the CMIP5, Clim. Dynam., 42, 101–119, 2014. 5398

Lejeune, Y., Bertrand, J.-M., Wagnon, P., and Morin, S.: A physically based model of the year-round surface energy and mass balance of debris-covered glaciers, J. Glaciol., 59, 327–344, doi:10.3189/2013JoG12J149, 2013. 5377

Liu, Y., Hou, S., Wang, Y., and Song, L.: Distribution of borehole temperature at four high-altitude alpine glaciers in central Asia, J. Mt. Sci., 6, 221–227, 2009. 5384

Lutz, A. F., Immerzeel, W. W., Gobiet, A., Pellicciotti, F., and Bierkens, M. F. P.: Comparison of climate change signals in CMIP3 and CMIP5 multi-model ensembles and implications for Central Asian glaciers, Hydrol. Earth Syst. Sci., 17, 3661–3677, doi:10.5194/hess-17-3661-2013, 2013. 5379, 5380

TCD
8, 5375–5432, 2014

Mae, S., Wushiki, H., Ageta, Y., and Higuchi, K.: Thermal drilling and temperature measurements in Khumbu Glacier, Nepal Himalayas, Seppyo, 37, 161–169, 1975. 5384
Marzeion, B., Jarosch, A. H., and Hofer, M.: Past and future sea-level change from the surface mass balance of glaciers, The Cryosphere, 6, 1295–1322, doi:10.5194/tc-6-1295-2012, 2012. 5395, 5399
Mathison, C., Wiltshire, A., Dimri, A., Falloon, P., Jacob, D., Kumar, P., Moors, E., Ridley, J., Siderius, C., Stoffel, M., and Yasunari, T.: Regional projections of North Indian climate for adaptation studies, Sci. Total Environ., 468–469, S4–S17, doi:10.1016/j.scitotenv.2012.04.066, 2013. 5381
Mirza, M., Warrick, R., Ericksen, N., and Kenny, G.: Trends and persistence in precipitation in the Ganges, Brahmaputra and Meghna river basins, Hydrolog. Sci. J., 43, 845–858, 1998. 5380
Mölg, T., Chiang, J. C. H., Gohm, A., and Cullen, N. J.: Temporal precipitation variability versus altitude on a tropical high mountain: observations and mesoscale atmospheric modelling, Q. J. Roy. Meteorol. Soc., 135, 1439–1455, doi:10.1002/qj.461, 2009. 5383
Mölg, T., Maussion, F., Yang, W., and Scherer, D.: The footprint of Asian monsoon dynamics in the mass and energy balance of a Tibetan glacier, The Cryosphere, 6, 1445–1461, doi:10.5194/tc-6-1445-2012, 2012. 5380, 5395
Naito, N., Nakawo, M., Kadota, T., and Raymond, C. F.: Numerical simulation of recent shrinkage of Khumbu Glacier, Nepal Himalayas, in: Debris-Covered Glaciers: Proceedings of an International Workshop Held at the University of Washington in Seattle, Washington, USA, 13–15 September 2000, vol. 264, International Association of Hydrological Sciences, 245 pp., 2000. 5380, 5398
Nakawo, M., Yabuki, H., and Sakai, A.: Characteristics of Khumbu Glacier, Nepal Himalaya: recent change in the debris-covered area, Ann. Glaciol., 28, 118–122, 1999. 5380, 5387
Nepal, S., Krause, P., Flügel, W.-A., Fink, M., and Fischer, C.: Understanding the hydrological system dynamics of a glaciated alpine catchment in the Himalayan region using the J2000 hydrological model, Hydrol. Process., 28, 1329–1344, doi:10.1002/hyp.9627, 2014. 5380, 5397, 5401
Nicholson, L. and Benn, D. I.: Calculating ice melt beneath a debris layer using meteorological data, J. Glaciol., 52, 463–470, doi:10.3189/172756506781828584, 2006. 5398

TCD
8, 5375–5432, 2014

Nuimura, T., Fujita, K., Yamaguchi, S., and Sharma, R. R.: Elevation changes of glaciers revealed by multitemporal digital elevation models calibrated by GPS survey in the Khumbu region, Nepal Himalaya, 1992–2008, J. Glaciol., 58, 648–656, doi:10.3189/2012JoG11J061, 2012. 5378, 5387, 5414

Oerlemans, J. and Fortuin, J. P. F.: Sensitivity of glaciers and small ice caps to greenhouse warming, Science, 258, 115–117, 1992. 5379, 5384

Ohmura, A.: Enhanced temperature variability in high-altitude climate change, Theor. Appl. Climatol., 110, 499–508, doi:10.1007/s00704-012-0687-x, 2012. 5379

Palazzi, E., Hardenberg, J., and Provenzale, A.: Precipitation in the Hindu-Kush Karakoram Himalaya: observations and future scenarios, J. Geophys. Res.-Atmos., 118, 85–100, doi:10.1029/2012JD018697, 2013. 5380, 5381

Pellicciotti, F., Buergi, C., Immerzeel, W., Konz, M., and Shrestha, A.: Challenges and uncertainties in hydrological modeling of remote Hindu Kush-Karakoram-Himalayan (HKH) basins: suggestions for calibration strategies, Mt. Res. Dev., 32, 39–50, doi:10.1659/MRD-JOURNAL-D-11-00092.1, 2012. 5390

Qi, W., Zhang, Y., Gao, J., Yang, X., Liu, L., and Khanal, N. R.: Climate change on the southern slope of Mt. Qomolangma (Everest) region in Nepal since 1971, J. Geogr. Sci., 23, 595–611, 2013. 5379, 5380, 5389

Quincey, D. J., Luckman, A., and Benn, D.: Quantification of Everest region glacier velocities between 1992 and 2002, using satellite radar interferometry and feature tracking, J. Glaciol., 55, 596–606, doi:10.3189/002214309789470987, 2009. 5387, 5414

Racoviteanu, A., Armstrong, R., and Williams, M.: Evaluation of an ice ablation model to estimate the contribution of melting glacier ice to annual discharge in the Nepalese Himalaya, Water Resour. Res., 49, 5117–5133, doi:10.1002/wrcr.20370, 2013. 5376, 5380

Radić, V. and Hock, R.: Regional and global volumes of glaciers derived from statistical upscaling of glacier inventory data, J. Geophys. Res.-Earth, 115, F01010, doi:10.1029/2009JF001373, 2010. 5386

Radić, V., Bliss, A., Beedlow, A. C., Hock, R., Miles, E., and Cogley, J. G.: Regional and global projections of twenty-first century glacier mass changes in response to climate scenarios from global climate models, Clim. Dynam., 42, 37–58, doi:10.1007/s00382-013-1719-7, 2014. 5395, 5399

TCD
8, 5375–5432, 2014

Rangwala, I. and Miller, J.: Climate change in mountains: a review of elevation-dependent warming and its possible causes, Climatic Change, 114, 527–547, doi:10.1007/s10584-012-0419-3, 2012. 5379

Rangwala, I., Miller, J. R., Russell, G. L., and Xu, M.: Using a global climate model to evaluate the influences of water vapor, snow cover and atmospheric aerosol on warming in the Tibetan Plateau during the twenty-first century, Clim. Dynam., 34, 859–872, doi:10.1007/s00382-009-0564-1, 2009. 5379

Rasmussen, L. A.: Meteorological controls on glacier mass balance in High Asia, Ann. Glaciol., 54, 352–359, doi:10.3189/2013AoG63A353, 2013. 5380

Reid, T. D. and Brock, B. W.: An energy-balance model for debris-covered glaciers including heat conduction through the debris layer, J. Glaciol., 56, 903–916, doi:10.3189/002214310794457218, 2010. 5377

Richardson, S. D. and Reynolds, J. M.: An overview of glacial hazards in the Himalayas, Quatern. Int., 65, 31–47, 2000. 5378

Salerno, F., Buraschi, E., Bruccoleri, G., Tartari, G., and Smiraglia, C.: Glacier surface-area changes in Sagarmatha national park, Nepal, in the second half of the 20th century, by comparison of historical maps, J. Glaciol., 54, 738–752, doi:10.3189/002214308786570926, 2008. 5378

Scherler, D., Bookhagen, B., and Strecker, M. R.: Hillslope-glacier coupling: the interplay of topography and glacial dynamics in High Asia, J. Geophys. Res.-Earth, 116, F02019, doi:10.1029/2010JF001751, 2011. 5385

Shi, Y. and Liu, S.: Estimation on the response of glaciers in China to the global warming in the 21st century, Chinese Sci. Bull., 45, 668–672, doi:10.1007/BF02886048, 2000. 5380

Shrestha, A. B. and Aryal, R.: Climate change in Nepal and its impact on Himalayan glaciers, Reg. Environ. Change, 11, 65–77, doi:10.1007/s10113-010-0174-9, 2011. 5379, 5386

Shrestha, A. B., Wake, C. P., Mayewski, P. A., and Dibb, J. E.: Maximum temperature trends in the Himalaya and its vicinity: an analysis based on temperature records from Nepal for the period 1971–94, J. Climate, 12, 2775–2786, doi:10.1175/1520-0442(1999)012<2775:MTTITH>2.0.CO;2, 1999. 5379

Shrestha, D., Singh, P., and Nakamura, K.: Spatiotemporal variation of rainfall over the central Himalayan region revealed by TRMM Precipitation Radar, J. Geophys. Res.-Atmos., 117, D22106, doi:10.1029/2012JD018140, 2012. 5397

TCD
8, 5375–5432, 2014

Singh, P., Kumar, N., Ramasastri, K., and Singh, Y.: Influence of a fine debris layer on the melting of snow and ice on a Himalayan Glacier, in: Debris Covered Glaciers, vol. 264 of IAHS Proceedings, IAHS, Wallingford, 63–69, 2000. 5391

Stahl, K. and Moore, R. D.: Influence of watershed glacier coverage on summer streamflow in British Columbia, Canada, Water Resour. Res., 42, W06201, doi:10.1029/2006WR005022, 2006. 5381

Thakuri, S., Salerno, F., Smiraglia, C., Bolch, T., D'Agata, C., Viviano, G., and Tartari, G.: Tracing glacier changes since the 1960s on the south slope of Mt. Everest (central Southern Himalaya) using optical satellite imagery, The Cryosphere, 8, 1297–1315, doi:10.5194/tc-8-1297-2014, 2014. 5395

Thompson, S. S., Benn, D. I., Dennis, K., and Luckman, A.: A rapidly growing moraine-dammed glacial lake on Ngozumpa Glacier, Nepal, Geomorphology, 145, 1–11, doi:10.1016/j.geomorph.2011.08.015, 2012. 5378

Turner, A. and Annamalai, H.: Climate change and the South Asian summer monsoon, Nat. Clim. Change, 2, 587–595, doi:10.1038/nclimate1495, 2012. 5399

Viviroli, D., Dürr, H. H., Messerli, B., Meybeck, M., and Weingartner, R.: Mountains of the world, water towers for humanity: typology, mapping, and global significance, Water Resour. Res., 43, W07447, doi:10.1029/2006WR005653, 2007. 5376

Wagnon, P., Vincent, C., Arnaud, Y., Berthier, E., Vuillermoz, E., Gruber, S., Ménégoz, M., Gilbert, A., Dumont, M., Shea, J. M., Stumm, D., and Pokhrel, B. K.: Seasonal and annual mass balances of Mera and Pokalde glaciers (Nepal Himalaya) since 2007, The Cryosphere, 7, 1769–1786, doi:10.5194/tc-7-1769-2013, 2013. 5377, 5379, 5383, 5388, 5392, 5393, 5428

Weertman, J.: On the sliding of glaciers, J. Glaciol., 3, 33–38, 1957. 5384

Williams, V. S.: Present and former equilibrium-line altitudes near Mount Everest, Nepal and Tibet, Arctic Alpine Res., 15, 201–211, 1983. 5379, 5392

Yao, T., Thompson, L., Yang, W., Yu, W., Gao, Y., Guo, X., Yang, X., Duan, K., Zhao, H., Xu, B., Pu, J., Lu, A., Xiang, Y., Kattel, D., and Joswiak, D.: Different glacier status with atmospheric circulations in Tibetan Plateau and surroundings, Nat. Clim. Change, 2, 663–667, doi:10.1038/NCLIMATE1580, 2012. 5378

Yatagai, A., Arakawa, O., Kamiguchi, K., Kawamoto, H., Nodzu, M. I., and Hamada, A.: A 44-year daily gridded precipitation dataset for Asia based on a dense network of rain gauges, Sola, 5, 137–140, doi:10.2151/sola.2009-035, 2009. 5381

TCD
8, 5375–5432, 2014

Yatagai, A., Kamiguchi, K., Arakawa, O., Hamada, A., Yasutomi, N., and Kitoh, A.: APHRODITE: constructing a long-term daily gridded precipitation dataset for asia based on a dense network of rain gauges, B. Am. Meteorol. Soc., 93, 1401–1415, doi:10.1175/BAMS-D-11-00122.1, 2012. 5381, 5382

Zhang, T., Xiao, C., Colgan, W., Qin, X., Du, W., Sun, W., Liu, Y., and Ding, M.: Observed and modelled ice temperature and velocity along the main flowline of East Rongbuk Glacier, Qomolangma (Mount Everest), Himalaya, J. Glaciol., 59, 438–448, doi:10.3189/2013JoG12J202, 2013. 5380

TCD
8, 5375–5432, 2014

Table 1. EVK2CNR meteorological stations used to validate downscaled APHRODITE temperature and precipitation fields.

Site	Latitude (°)	Longitude (°)	Elevation (m)
Lukla	27.69556	86.72306	2660
Namche	27.80239	86.71456	3570
Pheriche	27.89536	86.81875	4260
Pyramid	27.95903	86.81322	5035

TCD
8, 5375–5432, 2014

Table 2. Fixed and calibrated model parameters, with initial values, range, and final calibrated values. Degree day factors varied within 1 SD (Supplement Immerzeel et al., 2010).

Parameter	Description	Units	Initial value	Range	Calibrated value
ρ	Ice density	$kg\,m^{-3}$	916.7	–	–
g	gravitational acceleration	$m\,s^{-2}$	9.81	–	–
τ_0	Equilibrium shear stress	$N\,m^{-2}$	80 000	–	–
ν	Bedrock roughness	unitless	0.1	–	–
T_S	Snow/rain limit	°C	0	–	–
γ_T	Daily vertical temperature gradient	$°C\,m^{-1}$	variable	–	–
C_{DOY}	Temperature bias correction	°C	variable	–	–
R_{exp}	Aspect dependence of ddf	unitless	0.2	–	–
β_{TH}	Threshold avalanching angle	°	50	–	–
R	Material roughness coefficient	$N\,m^{-2}\,s^{1/3}$	1.80×10^9	$\pm 5.00 \times 10^8$	1.51×10^9
ddf_C	clean ice melt factor	$mm\,°C^{-1}\,d^{-1}$	8.63	±1SD	9.7
ddf_D	debris-covered ice melt factor	$mm\,°C^{-1}\,d^{-1}$	3.34	±1SD	4.6
ddf_K	Khumbu glacier melt factor	$mm\,°C^{-1}\,d^{-1}$	6.7		8.6
ddf_S	snow melt factor	$mm\,°C^{-1}\,d^{-1}$	5.3	±1SD	5.4
Z_c	Height of precipitation maximum	m a.s.l.	6000	±500	6268

TCD
8, 5375–5432, 2014

Table 3. Scores (unitless) from the 20 calibration runs vs. independent calibration data. Calibration targets were observed extents of four large termini, basin-wide net mass balance of −0.40 m (Nuimura et al., 2012), total glacier area of 410 km^2 in 2010 (ICIMOD, 2011), and mean velocity of 10 m yr^{-1} on debris covered tongues (Quincey et al., 2009). Mean and SD (σ) of scores are provided at the bottom of the table, and scores for the selected run are in bold.

Run	Terminus extents	B_a	Total area	Velocity	Total score
1	0.20	0.46	0.04	3.44	1.33×10^{-2}
2	0.19	0.31	0.03	2.78	5.22×10^{-3}
3	0.19	0.26	0.01	0.34	1.05×10^{-4}
4	0.19	0.69	0.04	0.38	1.92×10^{-3}
5	**0.17**	**0.19**	**0.06**	**0.05**	$\mathbf{9.78 \times 10^{-5}}$
6	0.20	0.58	0.01	0.75	6.95×10^{-4}
7	0.18	0.23	0.09	0.10	3.48×10^{-4}
8	0.19	0.70	0.03	0.88	3.55×10^{-3}
9	0.20	0.46	0.05	3.13	1.35×10^{-2}
10	0.18	0.45	0.05	0.01	4.45×10^{-5}
11	0.18	0.24	0.05	0.47	1.00×10^{-3}
12	0.19	0.33	0.04	1.21	2.77×10^{-3}
13	0.19	0.52	0.04	0.08	3.61×10^{-4}
14	0.17	0.05	0.09	0.44	3.44×10^{-4}
15	0.19	0.39	0.00	0.08	1.58×10^{-5}
16	0.18	0.44	0.04	0.72	2.12×10^{-3}
17	0.18	0.36	0.06	0.02	9.24×10^{-5}
18	0.19	0.56	0.05	0.37	2.03×10^{-3}
19	0.19	0.46	0.02	0.36	4.89×10^{-4}
20	0.18	0.20	0.10	0.37	1.36×10^{-3}
Mean	0.19	0.39	0.04	0.80	2.47×10^{-3}
σ	0.01	0.17	0.03	1.02	3.89×10^{-3}

TCD
8, 5375–5432, 2014

Table 4. Projected meanm annual temperature and precipitation changes from 1961–1990 to 2021–2050, extracted from RCP4.5 and RCP8.5 CMIP5 runs. See Supplement from Immerzeel et al. (2013) for more information.

Scenario	Description	d*P* (%)	d*T* (°C)	Model	Ensemble
RCP4.5	Dry, Cold	−3.2	1.5	HADGEM2-CC	r1i1p1
RCP4.5	Dry, Warm	−2.3	2.4	MIROC-ESM	r1i1p1
RCP4.5	Wet, Cold	12.4	1.3	MRI-CGCM3	r1i1p1
RCP4.5	Wet, Warm	12.1	2.4	IPSL-CM5A-LR	r3i1p1
RCP8.5	Dry, Cold	−3.6	1.7	HADGEM2-CC	r1i1p1
RCP8.5	Dry, Warm	−2.8	3.1	IPSL-CM5A-LR	r2i1p1
RCP8.5	Wet, Cold	15.6	1.8	CSIRO-MK3-60	r1i1p1
RCP8.5	Wet, Warm	16.4	2.9	CAN-ESM2	r2i1p1

TCD
8, 5375–5432, 2014

Table 5. Mean ($\overline{x}$) and SD (σ) in percent modelled glacier volume change for RCP4.5 and RCP8.5 end-members at 2050 and 2100.

Scenario	$\overline{x}_{2050}$	σ_{2050}	$\overline{x}_{2100}$	σ_{2100}
RCP4.5	−45.4	9.0	−83.2	8.7
RCP8.5	−51.9	9.8	−88.7	7.3

TCD
8, 5375–5432, 2014

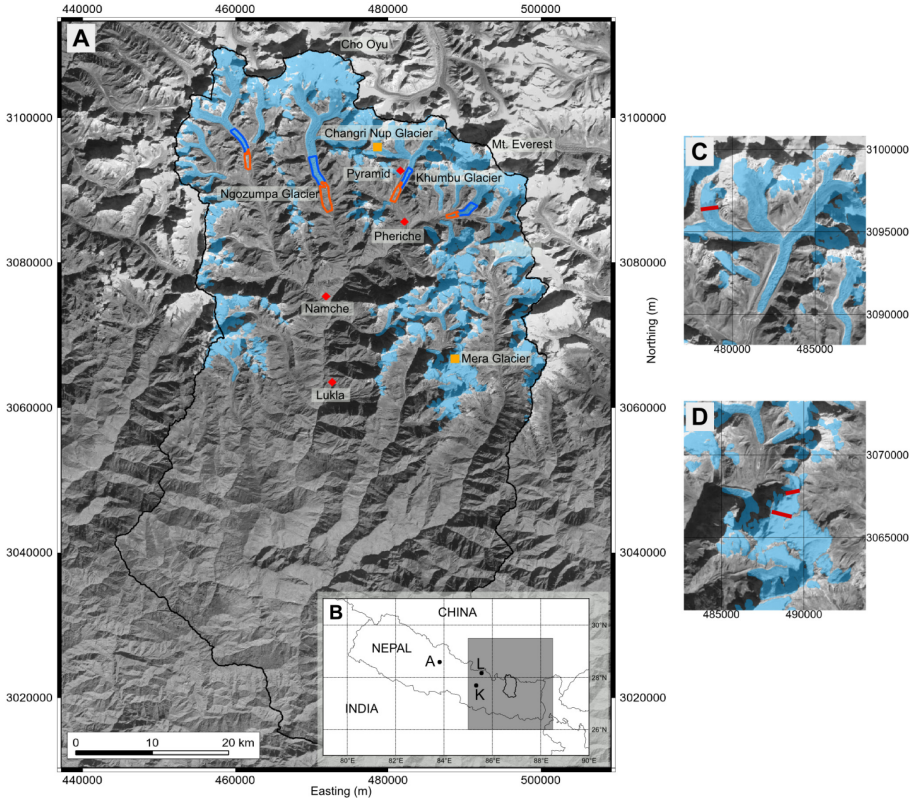

Figure 1. (a) Dudh Kosi basin, central Nepal, with current glacier extents in blue (ICIMOD, 2011), EVK2CNR stations (red), GPR profile sites (yellow). Extents of glacierized (blue) and non-glacierized (orange) regions used for model calibration are also shown. Coordinate system is UTM 45N. Inset map **(b)** shows the Dudh Kosi basin in relation to the APHRODITE subset (shaded), and the locations of places named in the text (A = Annapurna, L = Langtang, K = Kathmandu. **(c)** and **(d)** give the location of the transverse GPR surveys (thick red lines) at Changri Nup and Mera glaciers, respectively.

TCD
8, 5375–5432, 2014

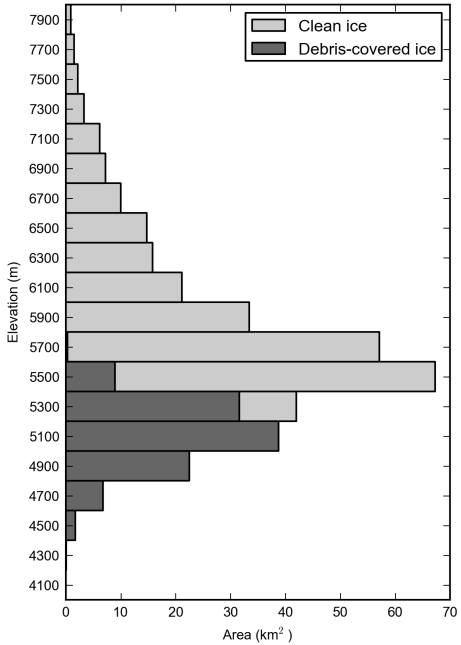

Figure 2. Area of clean and debris-covered glaciers by elevation, Dudh Kosi basin, Nepal. Extracted from SRTM 90 m DEM and glacier inventory from ICIMOD (2011).

TCD
8, 5375–5432, 2014

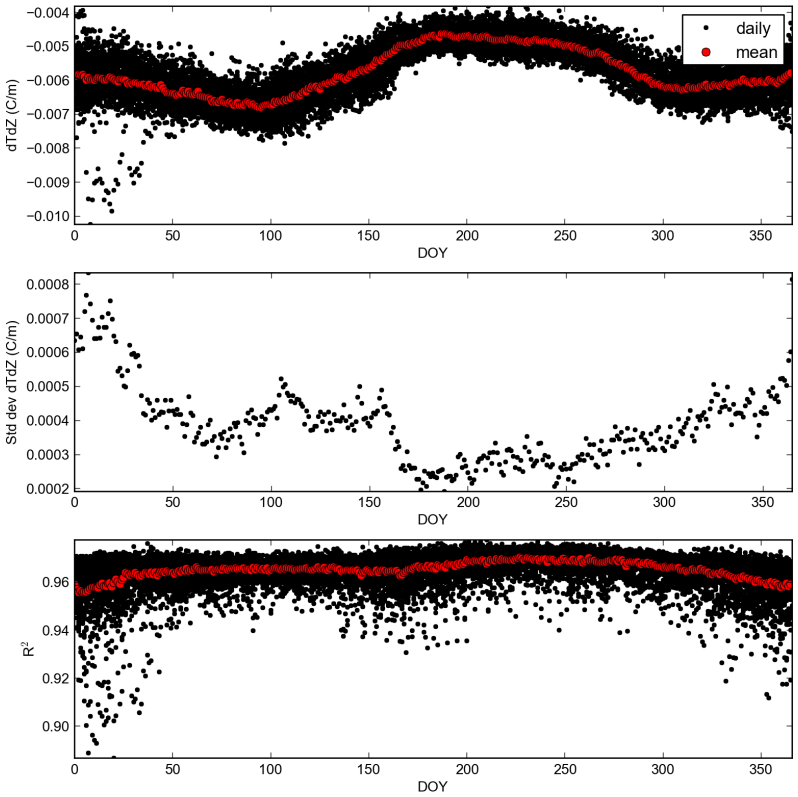

Figure 3. Top panel: vertical temperature gradients (γ_T) by day of year (DOY) for all years (black) calculated from APHRODITE (1961–2007) temperature fields and resampled SRTM data, with period mean for in red, middle panel: daily SD of γ_T, and bottom panel: mean daily coefficient of determination (R^2) calculated from the linear regression of resampled SRTM elevations and APRHODITE cell temperatures.

TCD
8, 5375–5432, 2014

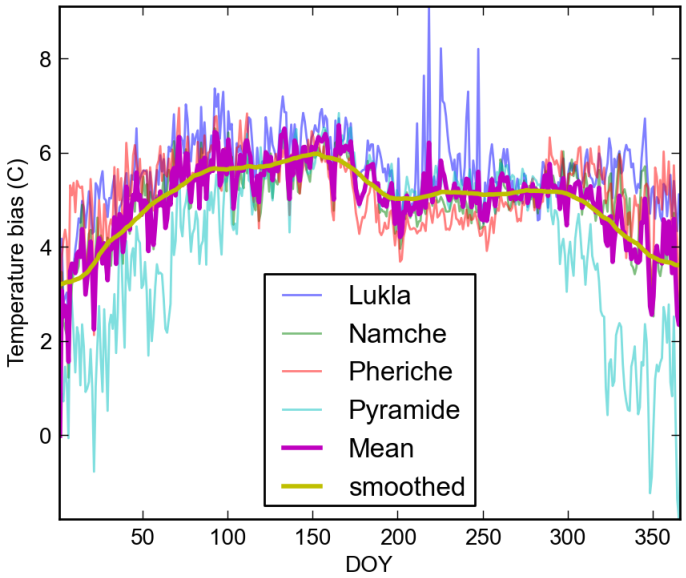

Figure 4. Average daily temperature bias (estimated–observed) for four EVK2CNR sites (2003–2007), their arithmetic mean, and a smoothed function used as a daily bias correction.

TCD
8, 5375–5432, 2014

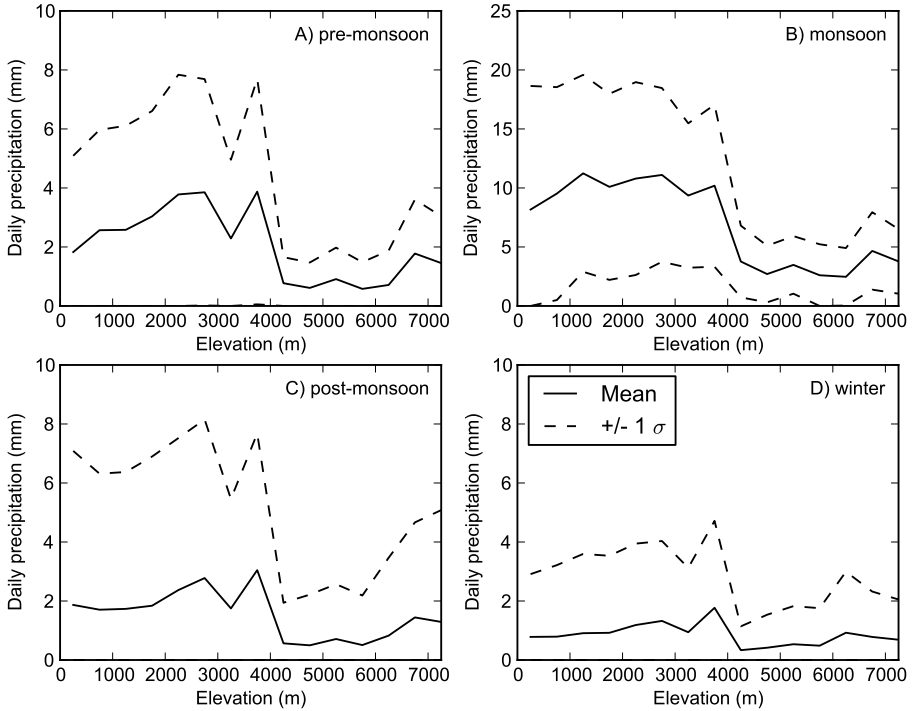

Figure 5. Mean and SD (σ) of APHRODITE (1961–2007) daily precipitation vs. elevation for pre-monsoon **(a)**, monsoon **(b)**, post-monsoon **(c)**, and winter **(d)**. Days with zero precipitation are excluded. Note different scale for **(b)**.

TCD
8, 5375–5432, 2014

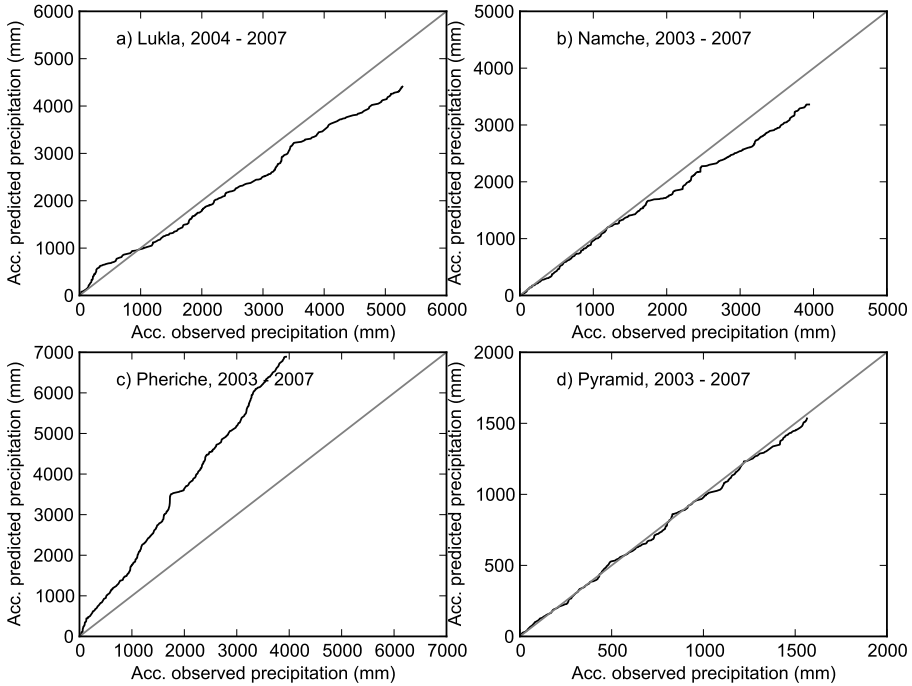

Figure 6. Accumulated observed and modelled precipitation at the EVK2CNR sites. Days where $T < 0$ or precipitation observations were missing were excluded from the analyses.

TCD
8, 5375–5432, 2014

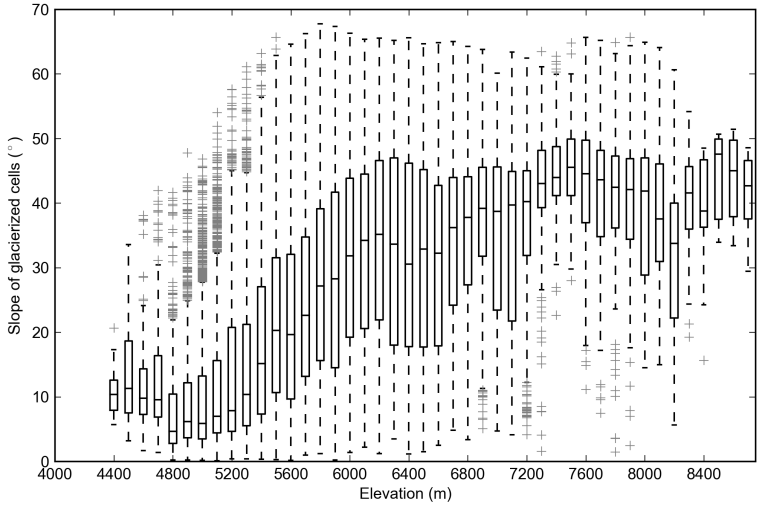

Figure 7. Boxplots of the slope of glacierized pixels in the Dudh Kosi basin, grouped by 100 m elevation bands. The boundaries of each box indicate the upper and lower quartiles, while the middle line of the box shows the median value. Whisker ends indicate the maximum (minimum) values excluding outliers, which are defined as more (less) than 3/2 times the upper (lower) quartile. Slope values were extracted from the SRTM 90 m DEM and glacier inventory from ICIMOD (2011).

TCD
8, 5375–5432, 2014

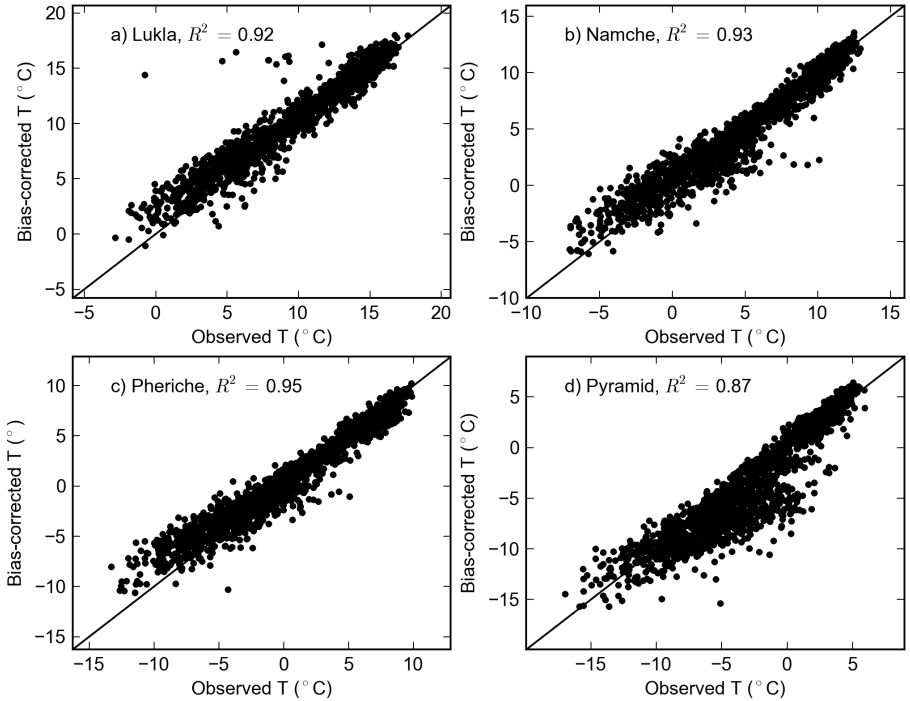

Figure 8. Mean daily temperatures observed at EVK2CNR sites (2003–2007) vs. bias-corrected temperatures estimated from APHRODITE temperature fields.

TCD
8, 5375–5432, 2014

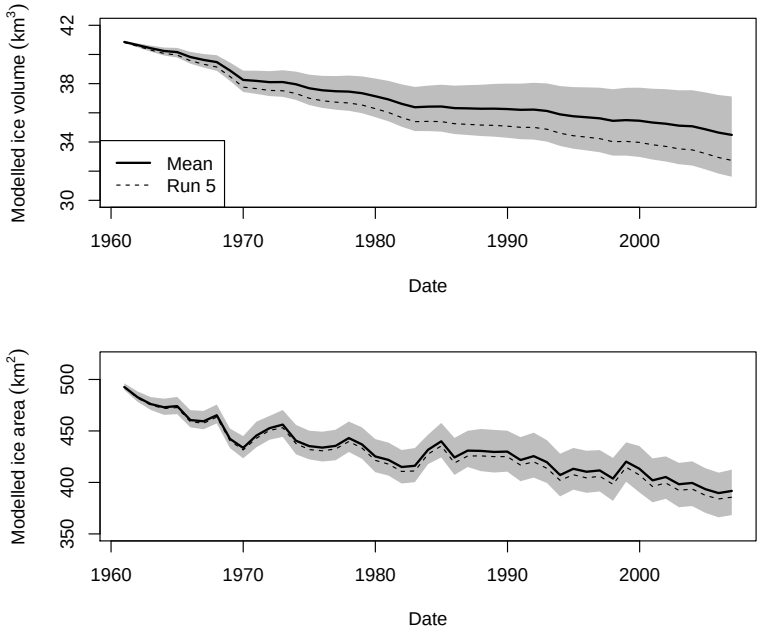

Figure 9. Top panel: modelled mean (1 November–31 January) ice volumes from the 20 calibration runs, 1961–2007, with multi-model mean (black line), minimum and maximum modelled volumes (shaded area), and results from Run 5 (dashed line). Bottom panel: as above, but for modelled glacier areas from the twenty calibration runs.

TCD
8, 5375–5432, 2014

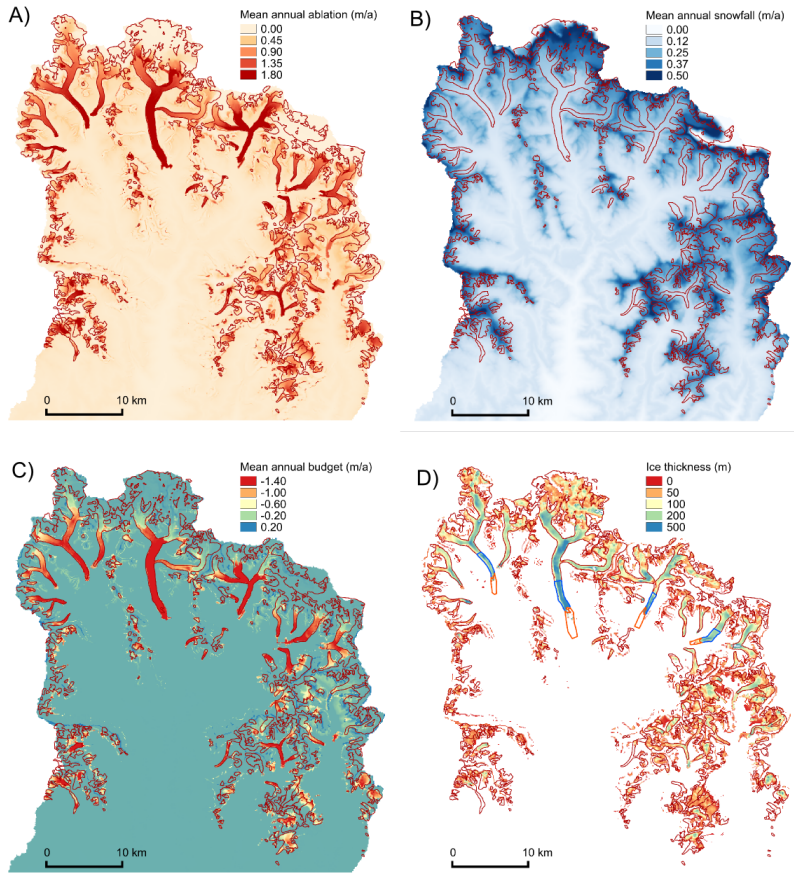

Figure 10. Results from the calibrated model run, 1961–2007. **(a)** Mean annual ablation, **(b)** mean annual snowfall, **(c)**, mean annual mass budget, **(d)** final ice thickness. Extents of glacierized and non-glacierized calibration regions are shown in **(d)**.

TCD
8, 5375–5432, 2014

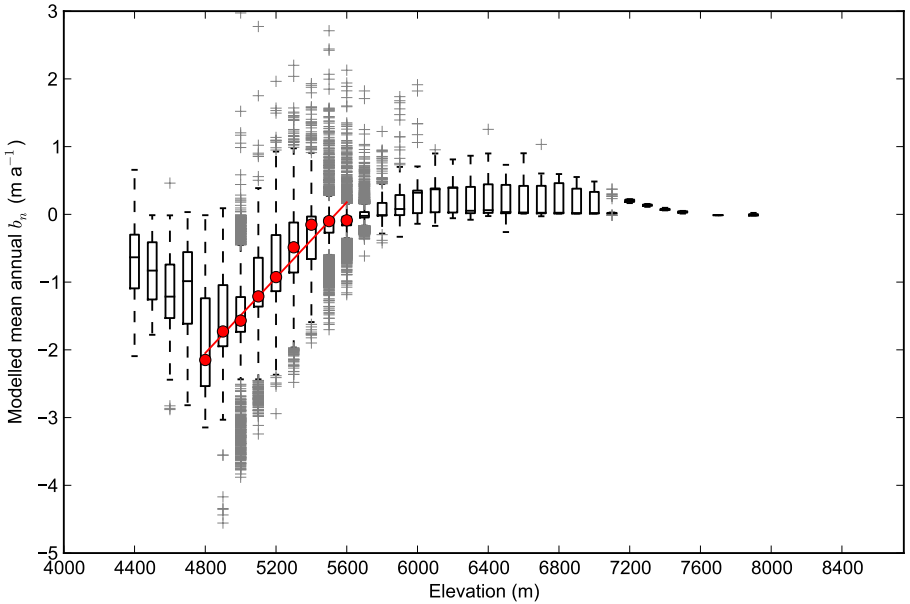

Figure 11. Boxplots of modelled mean annual mass balance (m w.e. yr^{-1}) calculated for 100 m intervals (1961–2007). Calculated mass balance gradient of 0.24 m (100 m)$^{-1}$ between 4850 and 5650 m is shown in red.

TCD
8, 5375–5432, 2014

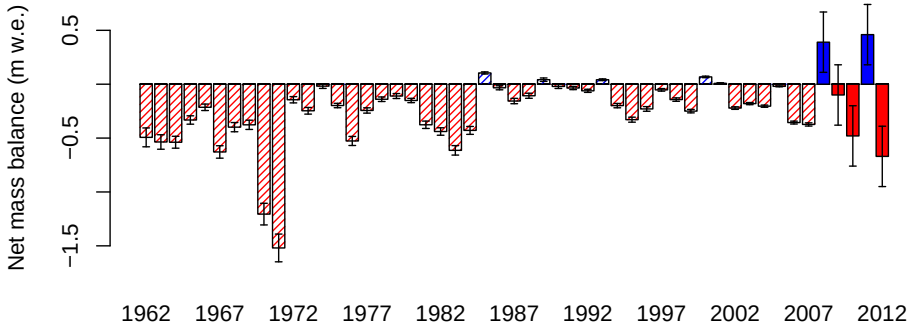

Figure 12. Modelled (dashed) and observed (solid) annual net mass balance at Mera Glacier, 1961–2007. Error bars for the modelled mass balances derived from the SD of the annual mass balances extracted from 20 calibration runs, and error bars for the observed mass balances are from Wagnon et al. (2013).

TCD
8, 5375–5432, 2014

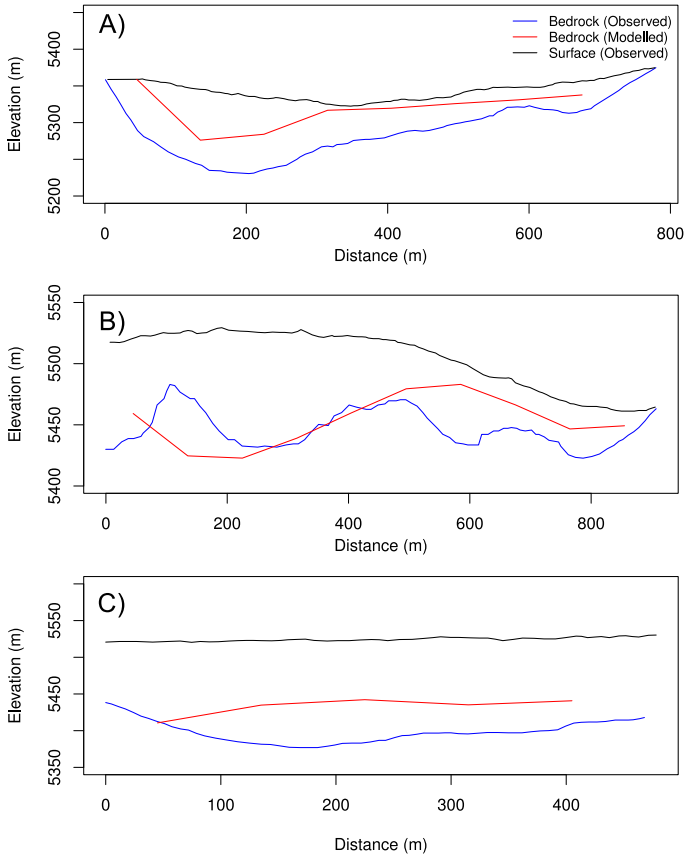

Figure 13. Glacier depths estimated from transverse ground-based GPR surveys and the mass balance and redistribution model, for **(a)** profile at 5350 m on Mera Glacier, **(b)** profile at 5540 m on Mera Glacier, and **(c)** profile at Changri Nup glacier.

TCD
8, 5375–5432, 2014

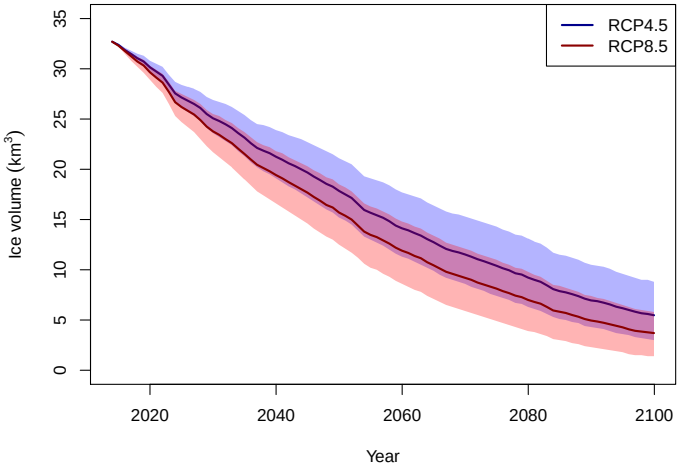

Figure 14. Variations in Dudh Kosi glacier volume response scenarios, for four RCP4.5 (blue) and four RCP8.5 (red) ensemble members (see Table 4 for details). Solid line represents the ensemble mean, and shaded area indicates minimum and maximum modelled ice volumes.

TCD
8, 5375–5432, 2014

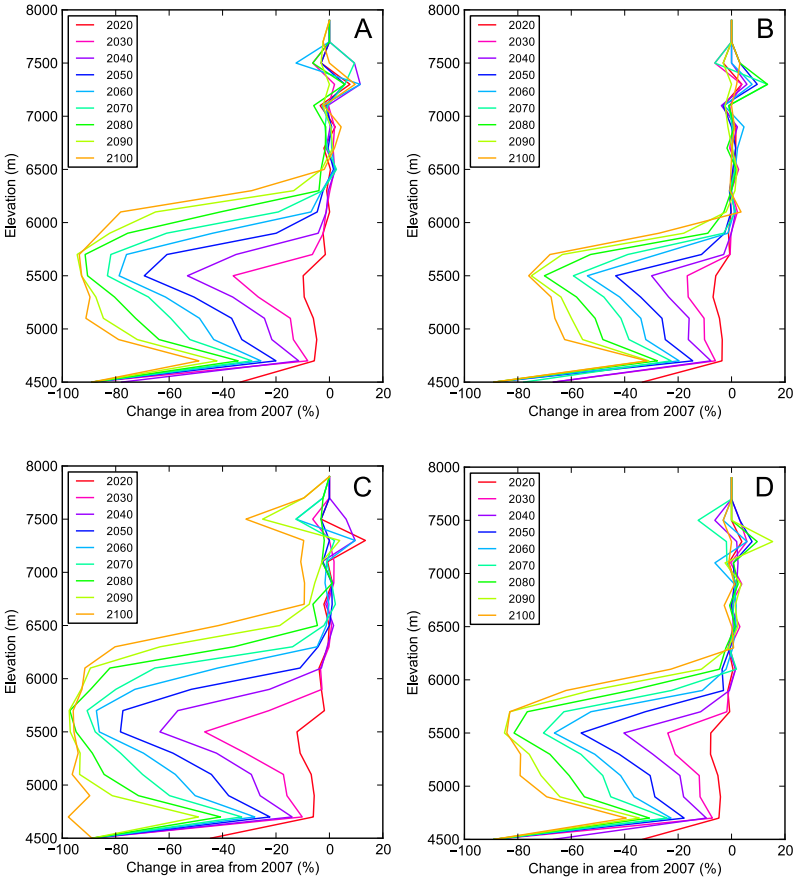

Figure 15. Modelled changes in glacier area from 2007 vs. elevation for **(a)** the dry/warm RCP4.5 scenario, **(b)** the wet/cool RCP4.5 scenario, **(c)** the dry/warm RCP8.5 scenario, and **(d)** the wet/cool RCP8.5 scenario.

TCD
8, 5375–5432, 2014

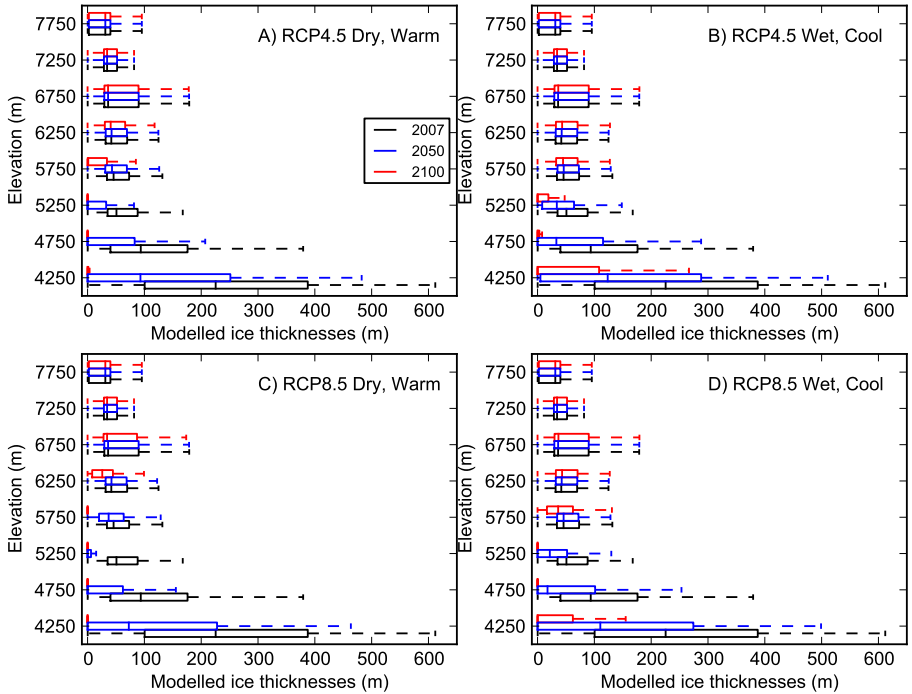

Figure 16. Distribution of modeled ice thicknesses by elevation band, for 2007 (initialization), 2050, and 2100. **(a)** Dry/warm RCMP4.5 scenario, **(b)**, wet/cool RCP4.5 scenario, **(c)** dry/warm RCP8.5 scenario, and **(d)** wet/cool RCP8.5 scenario.

TCD
8, 5375–5432, 2014